blood glucose levels began to increase as the expression of hepatic UCP1 declined. These findings indicate that hepatic UCP1 expression exerted therapeutic effects on diabetes associated with diet-induced obesity.

Resting oxygen consumption on day 3 was markedly increased, by 12%, in UCP1 mice compared with controls (Fig. 1*D*), whereas rectal temperature did not differ between the two (Fig. 1*E*). Thus, ectopic UCP1 in the liver, like endogenous UCP1 in brown adipocytes, promoted inefficient metabolism, thereby enhancing energy expenditure and leading to weight reduction. This effect, however, was not sufficient to raise whole-body temperature. In addition, hepatic UCP1 expression changed food intake. Whereas without hepatic UCP1 expression, food intake amounts in high-fat–fed mice were markedly increased compared with those in standard diet–fed lean mice (compare Figs. 1*F* and 5*D*), hepatic UCP1 expression reversed hyperphagia in mice with high-fat diet–induced obesity and diabetes (Fig. 1*F*). After day 8, concomitantly with the drop in hepatic UCP1 expression, hyperphagia was restored (Fig. 1*F*). In contrast, mice received an intravenous injection of adenovirus encoding CPT1a, another mitochondrial protein, did not show significantly altered food consumption (data not shown), suggesting that food intake suppression induced by hepatic UCP1 expression is not a nonspecific effect of expression of any of the hepatic mitochondrial proteins.

To eliminate any secondary effects of reduced food intake induced by hepatic UCP1 expression, we performed pair-feeding experiments. In contrast to UCP1 mice, pair-fed LacZ mice exhibited only slight decreases in body weights and blood glucose levels (of 3.1 and 6.9%, respectively, on day 7 after adenoviral administration). These results suggest that increased energy expenditure is an important mechanism underlying marked improvements of obesity and diabetes in UCP1 mice.

Hepatic UCP1 expression decreased fat contents in the liver and adipose tissues. Hepatic and adipose fat accumulations were examined on day 7 after adenoviral gene delivery. In the high-fat–fed control mice, liver weight and triglyceride content were markedly increased compared with the standard chow–fed lean mice (compare Fig. 2*A* and *B* with Fig. 5*E* and *F*, respectively). Hepatic UCP1 expression significantly decreased liver weight (Fig. 2*A*) and triglyceride content (Fig. 2*B*) compared with LacZ mice, with high-fat feeding. It is interesting that hepatic UCP1 expression also decreased fat content in their adipose tissues. For example, epididymal fat weight was significantly decreased in UCP1 mice compared with that in controls (Fig. 2*C*). Thus, hepatic expression of UCP1 exerts not only local effects in the liver but also remote effects on metabolism in other tissues.

These results were confirmed by the histological findings. No apparent infiltration or structural change was observed in the livers of either LacZ mice or UCP1 mice, indicating the absence of adenovirus-induced liver damage (Fig. 2*D*). Whereas abundant lipid droplets were present in the livers of control mice, these lipid droplets were markedly diminished in UCP1 mouse livers, indicating marked improvement of fatty liver findings in response to UCP1 expression (Fig. 2*D*). Furthermore, the cell diameters in epididymal fat (Fig. 2*E*) and brown adipose (Fig. 2*F*) tissues were significantly decreased in UCP1 mice. Expression levels of endogenous UCP1 protein in brown adipocytes were similar in the two groups (Fig. 2*G*), suggesting that energy expenditure in brown adipocytes was not increased in UCP1 mice. These findings suggest that hepatic UCP1 expression promotes hydrolysis of triglycerides already stored in adipose tissues, leading to smaller adipocytes with the resultant fatty acids being mobilized and metabolized as a substrate for oxidation in the liver.

Hepatic expressions of enzymes involved in lipid metabolism and glucose production. To elucidate the underlying mechanism whereby stored fat was decreased in the liver by hepatic UCP1 expression, we examined the expressions of proteins involved in lipid metabolism by quantitative RT-PCR. Significant reductions in the expressions of the lipogenic enzymes, including stearoyl-CoA desaturase-1 and fatty acid synthase, were observed in UCP1 mice (Fig. 3*A*). Sterol regulatory element binding protein 1c (SREBP1c) expression in the liver tended to be diminished. In contrast, hepatic expressions of enzymes involved in fatty acid oxidation tended to be increased. In particular, expressions of fatty acid transporter and UCP2 were significantly increased (Fig. 3*B*).

We further examined expression levels of key enzymes for hepatic glucose production. Hepatic phosphoenolpyruvate carboxykinase and glucose-6-phosphatase expressions were significantly decreased in UCP1 mice (Fig. 3*C*), suggesting a decrease to contribute to improvement of diabetes.

UCP1 expression may activate AMPK as a result of decreased generation of ATP. AMPK activation reportedly decreases malonyl-CoA generation via inhibition of ACC (21), resulting in enhancement of fatty acid oxidation. Therefore, ATP levels and AMPK phosphorylation in the liver were examined in LacZ and UCP1 mice under ad libitum feeding conditions. Hepatic ATP concentrations in UCP1 mice were approximately half those in control mice (Fig. 3*D*) but still ~2.3-fold those in standard diet–fed control mice. Hepatic AMPK activity was increased 1.6-fold in UCP1 mice compared with LacZ mice (Fig. 3*E*). The phosphorylation state of the α-subunit of AMPK in the liver was enhanced in UCP1 mice (Fig. 3*F*). Furthermore, resultant enhancement of hepatic ACC phosphorylation was observed (Fig. 3*G*). These findings suggest that AMPK activation induced by UCP1 expression plays an important role in the observed marked improvement of fatty liver findings via enhanced fatty acid oxidation.

Glucose and lipid metabolism in UCP1 mice. The results of oral glucose tolerance (Fig. 4*A*) and insulin tolerance (Fig. 4*B*) tests on day 7 after adenoviral administration clearly showed that hepatic expression of UCP1 markedly improved glucose tolerance and insulin sensitivity in obese and diabetic mice. Improved insulin sensitivity in muscle was confirmed by enhanced insulin receptor and IRS1 phosphorylation (Fig. 4*C*) in response to insulin administration. Thus, hepatic UCP1 expression exerts a remote beneficial effect on insulin sensitivity in muscle.

In addition, plasma lipid parameters were decreased in UCP1 mice. Total plasma cholesterol levels tended to be decreased in UCP1 mice compared with controls, although the changes were not statistically significant (Fig. 4*D*). Plasma triglyceride and free fatty acid levels were signifi-

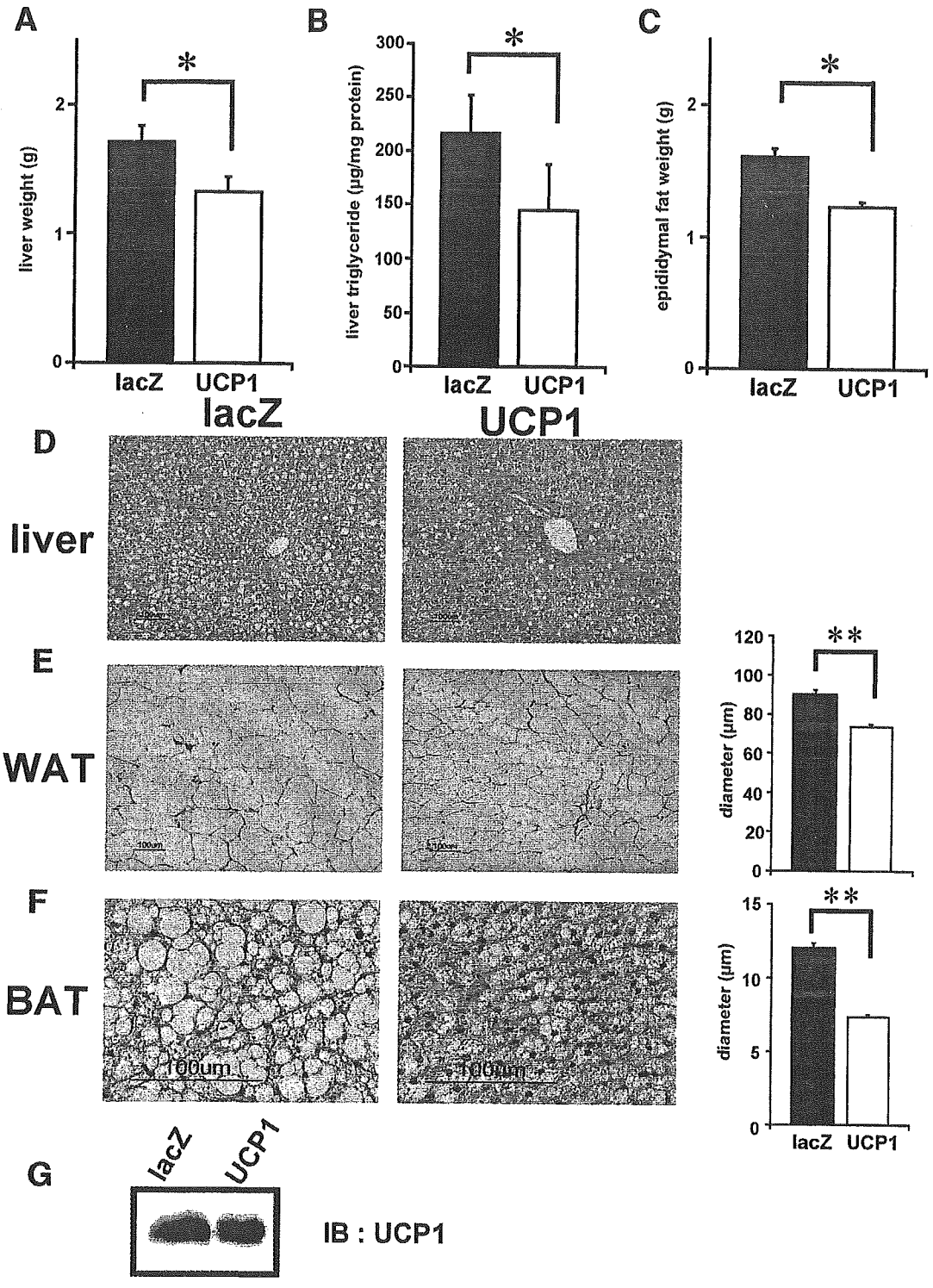

FIG. 2. Hepatic and adipose fat accumulations were decreased in UCP1 mice. Mice were killed after a 10-h fast on day 7 after adenoviral injection, and liver, epididymal fat (WAT), and brown adipose tissues (BAT) were removed. Liver weight (*A*), triglyceride content (*B*), and epididymal fat weight (*C*) were determined (n = 6 per group). *D–F*: Histological findings with hematoxylin and eosin (HE) staining of the liver (*D*), WAT (*E*), and BAT (*F*) in high-fat–fed control (*left*) and UCP1 mice (*middle*). In WAT (*E*) and BAT (*F*) tissues, cell diameters were measured (*right*). *G*: Endogenous UCP1 expression in BAT was compared between control (*left lane*) and UCP1 mice (*right lane*) by immunoblotting (n = 6 per group). Representative histological findings and immunoblots are presented. Data are presented as means ± SE. *P < 0.05, **P < 0.01 assessed by unpaired t test.

cantly decreased in UCP1 mice (Fig. 4*D*). Thus, hepatic UCP1 expression also improved diet-induced dyslipidemia.

Serum insulin levels were markedly decreased, by 57% (Fig. 4*E*), in UCP1 mice, despite lower blood glucose levels (Fig. 1*C*), indicating marked improvement of systemic insulin sensitivity. Serum adiponectin and TNF-α levels were similar in these groups (Fig. 4*F*), suggesting that these adipocytokines are not involved in the improvement of insulin resistance in UCP1 mice. In contrast, serum leptin levels were significantly decreased, by 56%, in

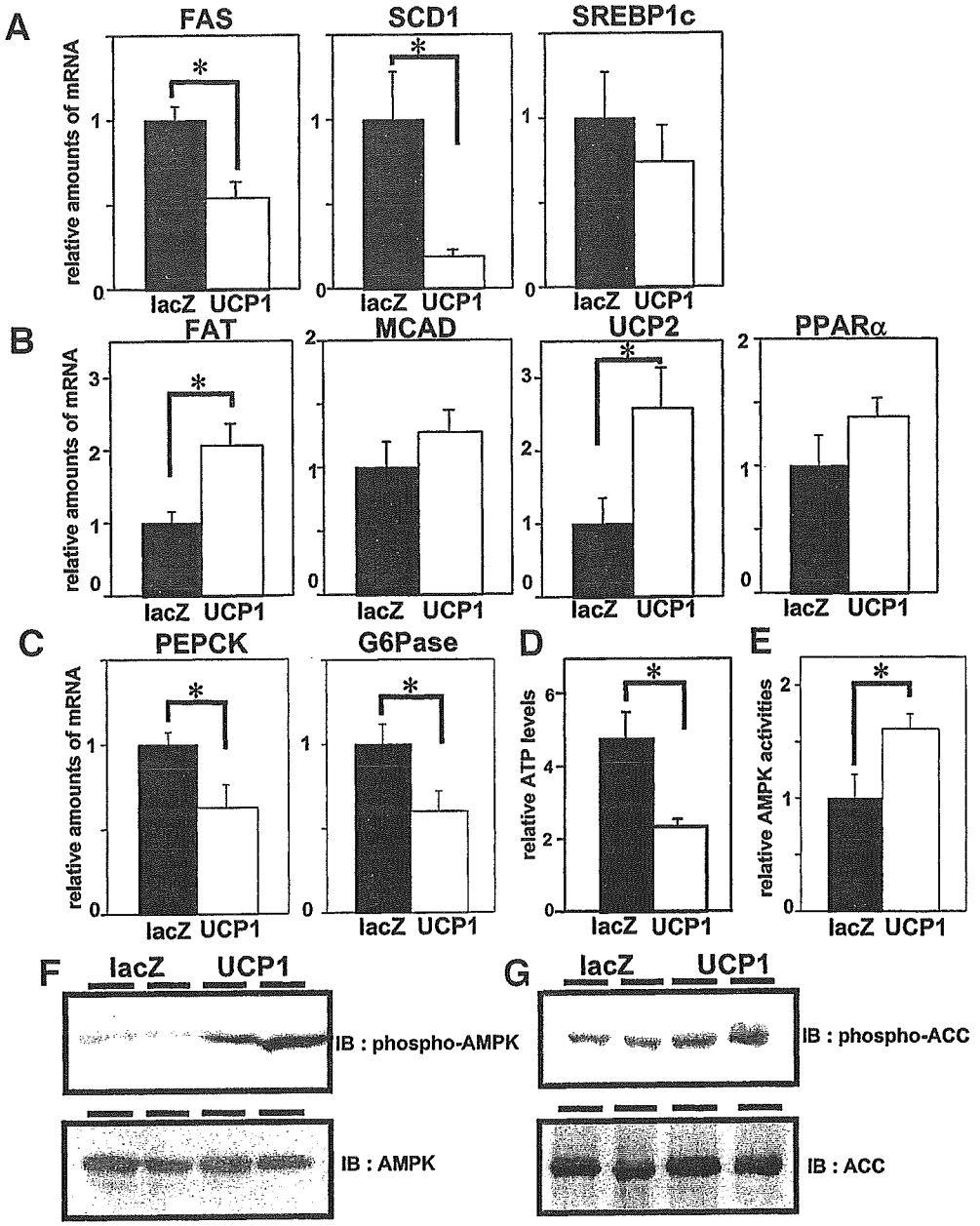

FIG. 3. Hepatic expressions of enzymes involved in lipid metabolism and glucose production and phosphorylations of AMPK and ACC. *A–C*: Relative amounts of mRNA were measured by quantitative RT-PCR and corrected with glyceraldehyde-3-dehydrogenase as the standard. Hepatic total RNA of mice, on day 3 after adenoviral administration in the 10-h–fasted state, was isolated. Expressions of lipogenic enzymes and SREBP1c (*A*), enzymes for fatty acid oxidation and PPAR-α (*B*), and enzymes for hepatic glucose production (*C*) in the liver were assayed (n = 6 per group). *D* and *E*: ATP concentrations (*D*) and AMPK activity (*E*) in the liver were measured. Data are presented as the relative amounts compared with those in standard diet–fed control mice (n = 6 per group). *F* and *G*: Immunoblots using anti–phospho-AMPK (*F*) or anti–phospho-ACC (*G*) antibody (*top*), as well as anti-AMPK (*F*) or anti-ACC1 (*G*) antibody (*bottom*) revealed the phosphorylation state of the AMPK α-subunit in the liver on day 3 after adenoviral injection (n = 2 per group). Data are presented as means ± SE. $^*P < 0.05$ assessed by unpaired t test.

UCP1 mice compared with those in control mice (Fig. 4*F*) concomitantly with decreased food intake (Fig. 1*F*). In control mice that were fed a high-fat diet, marked hyperleptinemia was observed (serum leptin concentrations, standard diet–fed mice versus high-fat diet–fed mice: 0.48 ± 0.08 vs. 32 0.8 ± 4.6 ng/ml) despite increased food intake (compare Fig. 1*F* with Fig. 5*D*), indicating leptin resistance. The present results suggest that hepatic UCP1 expression improves hypothalamic leptin resistance in obese and diabetic mice. To directly test whether leptin sensitivity was improved, we performed leptin tolerance tests (Fig. 4*G*). Leptin was injected intraperitoneally into fasted mice, followed by measurement of 12-h food intakes. The food intake inhibition by leptin administration was far more profound in UCP1 mice than in LacZ mice. Thus, UCP1 mice responded strongly to leptin administration, clearly showing that hepatic UCP1 expression exerts a therapeutic effect on hypothalamic leptin resistance.

Hepatic UCP1 expression exerted minimal effects in standard diet–fed lean mice. Hepatic UCP1 expression reduced body weight and blood glucose and lipid levels in obese and diabetic mice. These are very promising results suggesting that ectopic UCP1 expression may be useful in treating diabetic individuals who are obese. However, if

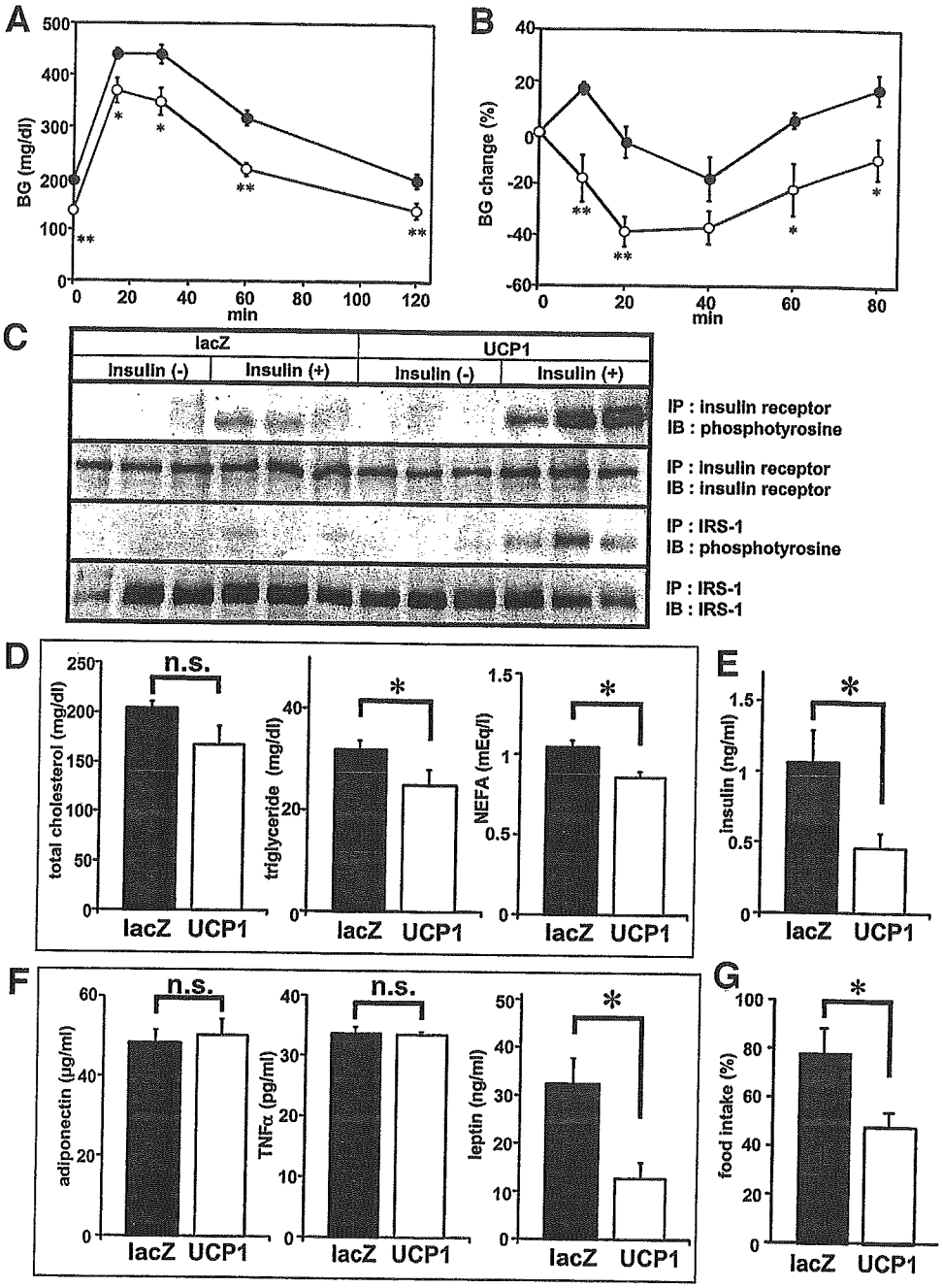

FIG. 4. Hepatic UCP1 expression improved glucose tolerance and insulin sensitivity. *A* and *B*: High-fat–fed mice on day 7 after adenoviral administration were subjected to glucose tolerance (*A*) and insulin tolerance (*B*) tests. Glucose tolerance tests were performed with an oral glucose load (2 g/kg body wt) after a 10-h fast. Insulin tolerance tests were performed in an ad libitum–fed state. Data were expressed as percentages of blood glucose levels immediately before intraperitoneal insulin loading (0.75 units/kg body wt). *C*: Insulin-stimulated tyrosine phosphorylation of insulin receptor and IRS1 proteins in muscle (n = 3 per group). Mice that were fasted for 16 h received an intravenous injection of 100 μl of normal saline with or without insulin (10 units/kg body wt). Hindlimb muscles were removed 300 s later, and lysates were immunoprecipitated with each antibody, as indicated. Immunoprecipitates were subjected to SDS-PAGE and immunoblotted with anti-phosphotyrosine antibody (4G10) or individual antibodies as indicated. *D–F*: Plasma lipid parameters (*D*; *left*, total cholesterol; *middle*, triglyceride; *right*, free fatty acids), serum insulin (*E*), and adipocytokines (*F*; *left*, adiponectin; *middle*, TNF-α; *right*, leptin) of high-fat–fed mice on day 7 after adenoviral administration were measured in the 10-h–fasted state. *G*: Leptin tolerance tests were performed on day 7 after adenoviral administration as described in RESEARCH DESIGN AND METHODS. Data were expressed as ratios to the food intake amounts of vehicle-treated mice (n = 6 per group). Data are presented as means ± SE. $^*P < 0.05$, $^{**}P < 0.01$ assessed by unpaired t test.

this were also the case in lean individuals, then these individuals would become leaner, possibly even developing malnutrition and hypoglycemia. We therefore performed experiments with a similar design but used 9-week-old standard diet–fed lean mice, i.e., the same age as the high-fat–fed mice.

It is intriguing that although ectopic UCP1 expression levels in the liver were similar under high-fat and standard diet conditions (Fig. 5*A*), the resultant phenotypes were completely different. In standard diet–fed lean mice, hepatic UCP1 expression did not alter body weight (Fig. 5*B*), fasting blood glucose levels (Fig. 5*C*), or food intake

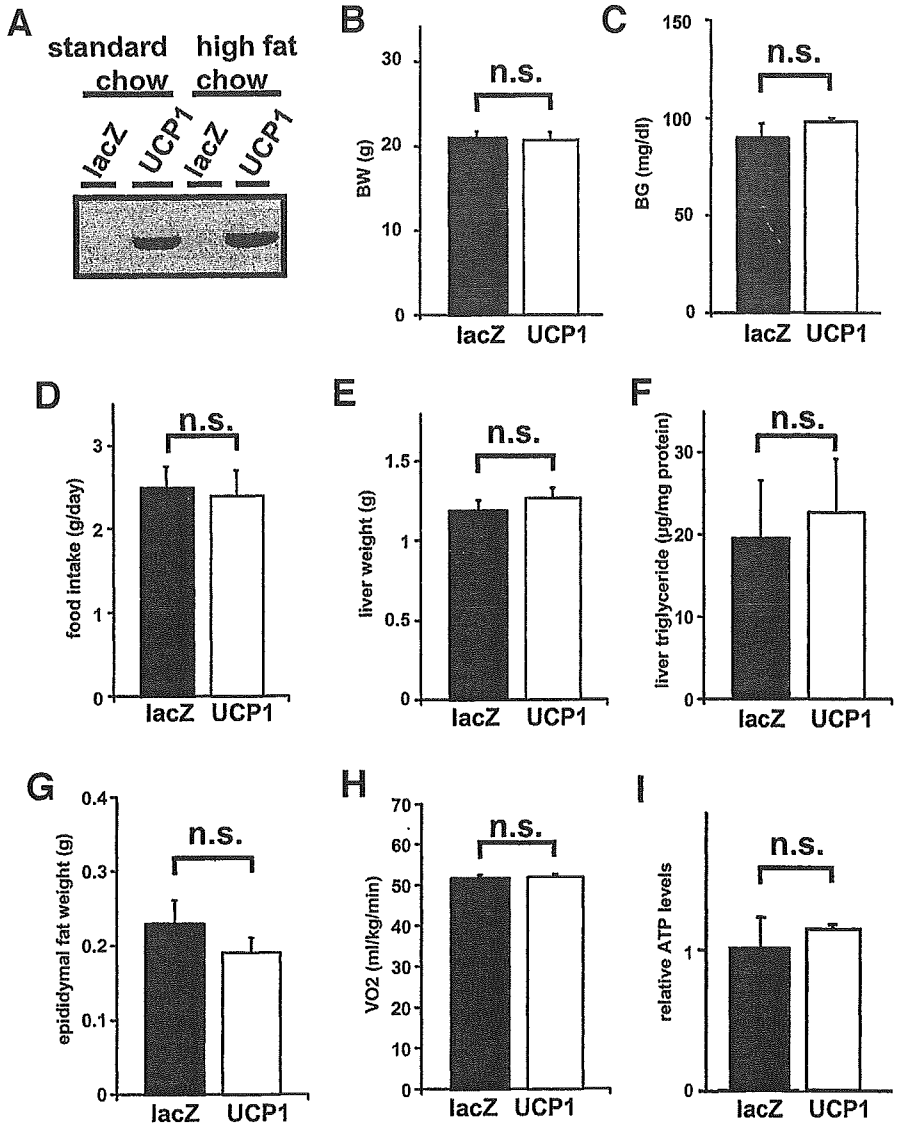

FIG. 5. Minimal effects of hepatic UCP1 expression in standard diet–fed lean mice. *A*: **Hepatic UCP1 expression in standard or high-fat diet–fed mice on day 7 after adenoviral administration at 9 weeks of age. Liver extracts from mice were immunoblotted using anti-UCP1 antibody.** *B* **and** *C*: **Body weights (*B*) and fasting blood glucose levels (*C*) were measured on day 7 after adenoviral injection.** *D*: **Food intake amounts were measured daily, and the average daily food intake for 7 days after adenoviral administration is represented.** *E–G*: **Hepatic weights (*E*), triglyceride contents (*F*), and epididymal fat weights (*G*) were determined (n = 6 per group) on day 7 after adenoviral injection.** *H* **and** *I*: **Resting Vo_2 (*H*) and hepatic ATP levels (*I*) were measured in the same way as in previous figures. Hepatic ATP levels are presented as the relative amounts compared with those in standard diet–fed control mice. Data are presented as means ± SE. **$P < 0.01$ assessed by one-factor ANOVA.**

amounts (Fig. 5*D*). In addition, hepatic weight (Fig. 5*E*), triglyceride content (Fig. 5*F*), and epididymal fat weight (Fig. 5*G*) were not changed. Thus, hepatic UCP1 expression did not exert significant effects on glucose metabolism or adiposity in lean mice.

To determine why hepatic UCP1 expression in lean mice did not significantly alter metabolic conditions, we measured basal energy expenditure and hepatic ATP contents. Hepatic UCP1 expression did not significantly change basal energy expenditure (Fig. 5*H*) or hepatic ATP levels (Fig. 5*I*), suggesting that UCP1 ectopically expressed in the liver is minimally involved in mitochondrial uncoupling, when surplus energy is not stored in the liver. Thus, hepatic UCP1 is likely to dissipate excess energy while having no effect on required energy. These characteristics are favorable in terms of therapeutic strategies for the metabolic syndrome.

DISCUSSION

In this study, after mice had developed obesity-associated diabetes, ectopically expressing UCP1 in the liver resulted in marked improvements in both disease conditions. UCP1 expression would be expected to decrease ATP generation in the liver and thus to activate hepatic AMPK. Indeed, ATP contents were decreased, and AMPK and ACC phosphorylations were increased. AMPK reportedly phosphorylates and inactivates ACC, resulting in a decrease in malonyl-CoA generation (21). Because malonyl-CoA is a negative regulator via suppression of CPT1, a rate-limiting enzyme for fatty acid oxidation (22), a decrease in malonyl-CoA generation is likely to enhance fatty acid oxidation to meet respiratory demands. Furthermore, hepatic expressions of lipogenic enzymes were decreased by UCP1 expression in the liver, which may be explained by

AMPK activation and possible SREBP1 reduction in the liver; metformin reportedly activates AMPK and inhibits hepatic SREBP1 expression (23). Taken together, the results suggest that fatty acid synthesis was suppressed with concomitant enhancement of fatty acid oxidation, resulting in the marked decrease in hepatic triglyceride contents.

How might a change in hepatic lipid metabolism affect the energy balance of the entire body? It is noteworthy that the weight and/or cell sizes of epididymal fat and brown adipose tissues were markedly decreased by hepatic UCP1 expression in the present study. Inhibition of fat accumulation in adipose tissues was also observed in UCP1 and in UCP3 transgenic mice under the control of muscle-specific promoters (7,8). Mice lacking ACC2, which is predominantly expressed in the heart and muscle of wild-type mice, also markedly inhibited fat accumulation in their adipose tissues (24). In reports using transgenic models, muscle is a site of increasing energy expenditure, through mitochondrial uncoupling, which prevents obesity. In the present study, hepatic expression of UCP1 reduced fat contents, rather than inhibiting fat accumulation, not only in the liver but also in adipose tissues, indicating promotion of hydrolysis of triglycerides already stored in the adipose tissues. Thus, hepatic uncoupling is likely to convey signals to peripheral adipose tissues. These signals might involve an autonomic nerve network, because the hydrolysis of triglycerides stored in adipose tissues is controlled mainly by the cAMP-mediated pathway, including sympathetic nerve activation (25). Alternatively, a decline in serum fatty acid concentrations, observed in UCP1 mice, or some unknown factors secreted by the liver might trigger lipolysis in adipose tissues. Although more work is required to elucidate the mechanism underlying this remote effect, enhancement of hepatic uncoupling is likely to exert therapeutic, rather than preventive, effects on insulin resistance associated with obesity. Thus, the liver is a potential therapeutic target for diabetes with obesity. Furthermore, unraveling the underlying mechanism may lead to development of antiobesity pharmacological agents that promote lipolysis in adipose tissues.

The present results are also interesting with respect to appetite regulation. Transgenic mice overexpressing UCP3 in skeletal muscle are reportedly hyperphagic (8), whereas UCP1 transgenic mice show no changes in food intake (7). In these transgenic mice, UCPs are continuously overexpressed throughout life, including in the fetal stage. In contrast, the UCP was expressed after development of diabetes with obesity in the present study. In obese subjects, serum leptin levels are reportedly increased with an increment in adipose tissue mass (26,27). Despite increased serum leptin levels, neither appetite nor food intake was suppressed, but instead increased, which is explained by hypothalamic leptin resistance in obese subjects. Herein, control mice on a high-fat diet were hyperphagic compared with those on a standard diet, whereas serum leptin levels were markedly elevated in high-fat diet–fed mice, indicating the development of leptin resistance. It is interesting that hepatic UCP1 expression reversed hyperphagia in high-fat diet–fed mice. Leptin tolerance tests show marked improvement of hypothalamic leptin resistance in UCP1 mice, another remote effect of hepatic UCP1 expression. In addition, increased fatty acid oxidation might be involved in the decreased food intake, because administration of peroxisome proliferator–activated receptor (PPAR)-α agonists reportedly reduces food intake amounts, but not in mice deficient in PPAR-α (28). Furthermore, streptozotocin-induced hyperphagia was reportedly reversed by hepatic expression of protein phosphatase-1 (29), suggesting that altering hepatic metabolism modulates appetite. Vagal pathways from the liver to the brain mediate the fat-induced changes in hypothalamic neuropeptides and feeding behavior in diabetic rats (30). Taken together with these observations, through appetite modulation, the liver also holds promise as a target for treatment of diabetes with obesity.

The most intriguing finding of the present study is that, despite similar UCP1 expression levels in mice on high-fat and standard diets, the resultant phenotypes were completely different. Hepatic UCP1 expression exerted no significant effects on food intake, weight change, or blood glucose levels in standard diet–fed lean mice. No alterations in energy expenditure or hepatic ATP contents were observed with hepatic UCP1 expression, indicating that, in the absence of a significant energy surplus, ectopic UCP1 has minimal effects on mitochondrial uncoupling. We performed similar experiments in a mildly obese and insulin-resistant model, 15% fat-fed mice. In these mice, hepatic UCP1 expression did not change body weight or food intake. Glucose tolerance and insulin sensitivity were significantly improved, but the effects were smaller (data not shown) than those in a more severely obese and insulin-resistant model, 32% fat-fed mice, reported here. Furthermore, under 32% high-fat–fed conditions in the present study, although hepatic UCP1 expression decreased ATP levels in the liver, the reduced ATP concentrations still exceeded those in standard diet–fed mice, suggesting that enhanced expression of UCPs in the liver does not itself produce an energy shortage. Taken together, hepatic UCP1 is likely to sense the metabolic state in the liver and function according to the degree of stored energy in the liver. In the reconstituted system, addition of fatty acids is indispensable for proton transport by UCP1 (31,32). Although the underlying mechanism has been widely debated (33,34), fatty acid cycling seems to be important for proton transport by UCP1 (35,36). Via such a mechanism, ectopic UCP1 activity in the liver may depend on the metabolic state, probably on the amount of stored fat in the liver. Thus, hepatic UCP1 seems to dissipate surplus energy but not to affect required energy. Therefore, the liver, in which intracellularly stored fat changes dramatically according to the energy balance, seems to be a good target tissue for enhanced expression of UCPs. This feature is of particular importance, as applied to therapeutic strategies for type 2 diabetes associated with obesity and insulin resistance.

Recently, it was reported that, using a transgenic technique, skeletal muscle expression of UCP1 in genetically obese mice lowers blood pressure (37), suggesting that uncoupling decreases the risk for atherosclerosis in patients with obesity and type 2 diabetes. In addition, uncoupling reportedly decreases the production of reactive oxygen species (38), although total oxygen consumption

increases. A high mitochondrial electrochemical gradient is associated with the production of reactive oxygen species that may damage tissues, a possible cause of diabetes complications and atherosclerosis (39). Thus, the respiratory uncoupling increment in the liver may protect tissues from oxidative stress. Taken together with the results of the present study, enhancement of UCPs in the liver is a potential therapy for the metabolic syndrome via reductions in adiposity and blood glucose levels as well as possibly reactive oxygen species in obese and diabetic individuals.

ACKNOWLEDGMENTS

This work was supported by a Grant-in-Aid for Scientific Research (B2, 15390282); a Grant-in-Aid for Exploratory Research (15659214); and Tohoku University 21st Century COE Program "Comprehensive Research and Education Center for Planning of Drug Development and Clinical Evaluation" to H.K. and a Grant-in-Aid for Scientific Research (13204062); and Tohoku University 21st Century COE Program "the Center for Innovative Therapeutic Development for Common Diseases" to Y.O. from the Ministry of Education, Science, Sports and Culture of Japan.

We thank Prof. Y. Moriyama (Okayama University) for helpful suggestions for measuring ATP. We also thank I. Sato and K. Kawamura for technical support.

REFERENCES

1. Friedman JM: A war on obesity, not the obese. *Science* 299:856–858, 2003
2. Klingenberg M, Huang SG: Structure and function of the uncoupling protein from brown adipose tissue. *Biochim Biophys Acta* 1415:271–296, 1999
3. Enerback S, Jacobsson A, Simpson EM, Guerra C, Yamashita H, Harper ME, Kozak LP: Mice lacking mitochondrial uncoupling protein are cold-sensitive but not obese. *Nature* 387:90–94, 1997
4. Himms-Hagen J: Brown adipose tissue thermogenesis and obesity. *Prog Lipid Res* 28:67–115, 1989
5. Kopecky J, Clarke G, Enerback S, Spiegelman B, Kozak LP: Expression of the mitochondrial uncoupling protein gene from the aP2 gene promoter prevents genetic obesity. *J Clin Invest* 96:2914–2923, 1995
6. Kopecky J, Hodny Z, Rossmeisl M, Syrovy I, Kozak LP: Reduction of dietary obesity in aP2-Ucp transgenic mice: physiology and adipose tissue distribution. *Am J Physiol* 270:E768–E775, 1996
7. Li B, Nolte LA, Ju JS, Han DH, Coleman T, Holloszy JO, Semenkovich CF: Skeletal muscle respiratory uncoupling prevents diet-induced obesity and insulin resistance in mice. *Nat Med* 6:1115–1120, 2000
8. Clapham JC, Arch JR, Chapman H, Haynes A, Lister C, Moore GB, Piercy V, Carter SA, Lehner I, Smith SA, Beeley LJ, Godden RJ, Herrity N, Skehel M, Changani KK, Hockings PD, Reid DG, Squires SM, Hatcher J, Trail B, Latcham J, Rastan S, Harper AJ, Cadenas S, Buckingham JA, Brand MD, Abuin A: Mice overexpressing human uncoupling protein-3 in skeletal muscle are hyperphagic and lean. *Nature* 406:415–418, 2000
9. Ono H, Shimano H, Katagiri H, Yahagi N, Sakoda H, Onishi Y, Anai M, Ogihara T, Fujishiro M, Viana AY, Fukushima Y, Abe M, Shojima N, Kikuchi M, Yamada N, Oka Y, Asano T: Hepatic Akt activation induces marked hypoglycemia, hepatomegaly, and hypertriglyceridemia with sterol regulatory element binding protein involvement. *Diabetes* 52:2905–2913, 2003
10. Kozak LP, Britton JH, Kozak UC, Wells JM: The mitochondrial uncoupling protein gene: correlation of exon structure to transmembrane domains. *J Biol Chem* 263:12274–12277, 1988
11. Nakazaki M, Kakei M, Ishihara H, Koriyama N, Hashiguchi H, Aso K, Fukudome M, Oka Y, Yada T, Tei C: Association of upregulated activity of K(ATP) channels with impaired insulin secretion in UCP1-expressing insulinoma cells. *J Physiol* 540:781–789, 2002
12. Katagiri H, Asano T, Ishihara H, Inukai K, Shibasaki Y, Kikuchi M, Yazaki Y, Oka Y: Overexpression of catalytic subunit p110α of phosphatidylinositol 3-kinase increases glucose transport activity with translocation of glucose transporters in 3T3-L1 adipocytes. *J Biol Chem* 271:16987–16990, 1996
13. Kanegae Y, Lee G, Sato Y, Tanaka M, Nakai M, Sakaki T, Sugano S, Saito I: Efficient gene activation in mammalian cells by using recombinant adenovirus expressing site-specific Cre recombinase. *Nucleic Acids Res* 23:3816–3821, 1995
14. Ikemoto S, Thompson KS, Takahashi M, Itakura H, Lane MD, Ezaki O: High fat diet-induced hyperglycemia: prevention by low level expression of a glucose transporter (GLUT4) minigene in transgenic mice. *Proc Natl Acad Sci U S A* 92:3096–3099, 1995
15. Ogihara T, Shin BC, Anai M, Katagiri H, Inukai K, Funaki M, Fukushima Y, Ishihara H, Takata K, Kikuchi M, Yazaki Y, Oka Y, Asano T: Insulin receptor substrate (IRS)-2 is dephosphorylated more rapidly than IRS-1 via its association with phosphatidylinositol 3-kinase in skeletal muscle cells. *J Biol Chem* 272:12868–12873, 1997
16. Folch J, Lees M, Sloane Stanley GH: A simple method for the isolation and purification of total lipides from animal tissues. *J Biol Chem* 226:497–509, 1957
17. Manfredi G, Yang L, Gajewski CD, Mattiazzi M: Measurements of ATP in mammalian cells. *Methods* 26:317–326, 2002
18. Sakoda H, Ogihara T, Anai M, Fujishiro M, Ono H, Onishi Y, Katagiri H, Abe M, Fukushima Y, Shojima N, Inukai K, Kikuchi M, Oka Y, Asano T: Activation of AMPK is essential for AICAR-induced glucose uptake by skeletal muscle but not adipocytes. *Am J Physiol Endocrinol Metab* 282:E1239–E1244, 2002
19. Igel M, Becker W, Herberg L, Joost HG: Hyperleptinemia, leptin resistance, and polymorphic leptin receptor in the New Zealand obese mouse. *Endocrinology* 138:4234–4239, 1997
20. Ishigaki Y, Oikawa S, Suzuki T, Usui S, Magoori K, Kim DH, Suzuki H, Sasaki J, Sasano H, Okazaki M, Toyota T, Saito T, Yamamoto TT: Virus-mediated transduction of apolipoprotein E (ApoE)-sendai develops lipoprotein glomerulopathy in ApoE-deficient mice. *J Biol Chem* 275: 31269–31273, 2000
21. Hardie DG: Regulation of fatty acid and cholesterol metabolism by the AMP-activated protein kinase. *Biochim Biophys Acta* 1123:231–238, 1992
22. McGarry JD, Brown NF: The mitochondrial carnitine palmitoyltransferase system: from concept to molecular analysis. *Eur J Biochem* 244:1–14, 1997
23. Zhou G, Myers R, Li Y, Chen Y, Shen X, Fenyk-Melody J, Wu M, Ventre J, Doebber T, Fujii N, Musi N, Hirshman MF, Goodyear LJ, Moller DE: Role of AMP-activated protein kinase in mechanism of metformin action. *J Clin Invest* 108:1167–1174, 2001
24. Abu-Elheiga L, Matzuk MM, Abo-Hashema KA, Wakil SJ: Continuous fatty acid oxidation and reduced fat storage in mice lacking acetyl-CoA carboxylase 2. *Science* 291:2613–2616, 2001
25. Londos C, Brasaemle DL, Schultz CJ, Adler-Wailes DC, Levin DM, Kimmel AR, Rondinone CM: On the control of lipolysis in adipocytes. *Ann N Y Acad Sci* 892:155–168, 1999
26. Maffei M, Halaas J, Ravussin E, Pratley RE, Lee GH, Zhang Y, Fei H, Kim S, Lallone R, Ranganathan S, et al.: Leptin levels in human and rodent: measurement of plasma leptin and ob RNA in obese and weight-reduced subjects. *Nat Med* 1:1155–1161, 1995
27. Considine RV, Sinha MK, Heiman ML, Kriauciunas A, Stephens TW, Nyce MR, Ohannesian JP, Marco CC, McKee LJ, Bauer TL, et al.: Serum immunoreactive-leptin concentrations in normal-weight and obese humans. *N Engl J Med* 334:292–295, 1996
28. Fu J, Gaetani S, Oveisi F, Lo Verme J, Serrano A, Rodriguez De Fonseca F, Rosengarth A, Luecke H, Di Giacomo B, Tarzia G, Piomelli D: Oleylethanolamide regulates feeding and body weight through activation of the nuclear receptor PPAR-alpha. *Nature* 425:90–93, 2003
29. Yang R, Newgard CB: Hepatic expression of a targeting subunit of protein phosphatase-1 in streptozotocin-diabetic rats reverses hyperglycemia and hyperphagia despite depressed glucokinase expression. *J Biol Chem* 278:23418–23425, 2003
30. la Fleur SE, Ji H, Manalo SL, Friedman MI, Dallman MF: The hepatic vagus mediates fat-induced inhibition of diabetic hyperphagia. *Diabetes* 52:2321–2330, 2003
31. Strieleman PJ, Schalinske KL, Shrago E: Fatty acid activation of the reconstituted brown adipose tissue mitochondria uncoupling protein. *J Biol Chem* 260:13402–13405, 1985
32. Winkler E, Klingenberg M: Effect of fatty acids on H+ transport activity of the reconstituted uncoupling protein. *J Biol Chem* 269:2508–2515, 1994
33. Klingenberg M, Echtay KS: Uncoupling proteins: the issues from a biochemist point of view. *Biochim Biophys Acta* 1504:128–143, 2001

34. Jezek P: Possible physiological roles of mitochondrial uncoupling proteins—UCPn. *Int J Biochem Cell Biol* 34:1190–1206, 2002
35. Skulachev VP: Fatty acid circuit as a physiological mechanism of uncoupling of oxidative phosphorylation. *FEBS Lett* 294:158–162, 1991
36. Garlid KD, Orosz DE, Modriansky M, Vassanelli S, Jezek P: On the mechanism of fatty acid-induced proton transport by mitochondrial uncoupling protein. *J Biol Chem* 271:2615–2620, 1996
37. Bernal-Mizrachi C, Weng S, Li B, Nolte LA, Feng C, Coleman T, Holloszy JO, Semenkovich CF: Respiratory uncoupling lowers blood pressure through a leptin-dependent mechanism in genetically obese mice. *Arterioscler Thromb Vasc Biol* 22:961–968, 2002
38. Vidal-Puig AJ, Grujic D, Zhang CY, Hagen T, Boss O, Ido Y, Szczepanik A, Wade J, Mootha V, Cortright R, Muoio DM, Lowell BB: Energy metabolism in uncoupling protein 3 gene knockout mice. *J Biol Chem* 275:16258–16266, 2000
39. Esposito LA, Melov S, Panov A, Cottrell BA, Wallace DC: Mitochondrial disease in mouse results in increased oxidative stress. *Proc Natl Acad Sci U S A* 96:4820–4825, 1999

Available online at www.sciencedirect.com
SCIENCE DIRECT®
Biochemical and Biophysical Research Communications 326 (2005) 402–409
BBRC
www.elsevier.com/locate/ybbrc

Constitutively active PDX1 induced efficient insulin production in adult murine liver

Junta Imai[a,b], Hideki Katagiri[b,*], Tetsuya Yamada[a], Yasushi Ishigaki[a], Takehide Ogihara[b], Kenji Uno[a,b], Yutaka Hasegawa[a,b], Junhong Gao[a,b], Hisamitsu Ishihara[a], Hironobu Sasano[c], Hiroyuki Mizuguchi[d], Tomoichiro Asano[e], Yoshitomo Oka[a]

[a] *Division of Molecular Metabolism and Diabetes, Tohoku University Graduate School of Medicine, Japan*
[b] *Division of Advanced Therapeutics for Metabolic Diseases, Center for Translational and Advanced Animal Research, Tohoku University Graduate School of Medicine, Japan*
[c] *Division of Anatomic Pathology, Tohoku University Graduate School of Medicine, Sendai 980-8575, Japan*
[d] *Division of Cellular and Gene Therapy Products, National Institute of Health Science, Tokyo, Japan*
[e] *Department of Physiological Chemistry and Metabolism, University of Tokyo, Tokyo 113-8655, Japan*

Received 21 October 2004
Available online 19 November 2004

Abstract

To generate insulin-producing cells in the liver, recombinant adenovirus containing a constitutively active mutant of PDX1 (PDX1-VP16), designed to activate target genes without the need for protein partners, was prepared and administered intravenously to streptozotocin (STZ)-treated diabetic mice. The effects were compared with those of administering wild-type PDX1 (wt-PDX1) adenovirus. Administration of these adenoviruses at 2×10^8 pfu induced similar levels of PDX1 protein expression in the liver. While wt-PDX1 expression exerted small effects on blood glucose levels, treatment with PDX1-VP16 adenovirus efficiently induced insulin production in hepatocytes, resulting in reversal of STZ-induced hyperglycemia. The effects were sustained through day 40 when exogenous PDX1-VP16 protein expression was undetectable in the liver. Endogenous PDX1 protein came to be expressed in the liver, which is likely to be the mechanism underlying the sustained effects. On the other hand, albumin and transferrin expressions were observed in insulin-producing cells in the liver, suggesting preservation of hepatocytic functions. Thus, transient expression of an active mutant of PDX1 in the liver induced sustained PDX1 and insulin expressions without loss of hepatocytic function.

Keywords: Insulin; PDX1; Gene therapy; Diabetes; Adenovirus; Transdifferentiation

Type 1 diabetes mellitus is characterized by progressive loss of pancreatic β cells, leading to a lifelong dependency on insulin treatments. Recently, marked advances have been made in transplanting pancreatic islets from human cadavers into type 1 diabetics [1]. However, immune rejection and donor supply are still major challenges in islet cell transplantation. In this context, generation of insulin-producing cells by somatic gene therapy may represent a viable alternative for the treatment for diabetes.

The liver is a possible target organ for generation of insulin-producing cells. Pancreatic and hepatic tissues both express several transcription factors such as HNF1α and C/EBPβ. In addition, these tissues also have similar glucose sensing machinery consisting of the GLUT2 glucose transporter and glucokinase. Furthermore, during embryogenesis, the liver and the ventral pancreas appear to arise from the same cell

* Corresponding author. Fax: +81 22 717 8228.
E-mail address: katagiri-tky@umin.ac.jp (H. Katagiri).

0006-291X/$ - see front matter © 2004 Elsevier Inc. All rights reserved.
doi:10.1016/j.bbrc.2004.11.047

population located within the embryonic endoderm [2]. The gene most likely to be responsible for the difference between the liver and pancreas is pancreatic and duodenal homeobox gene 1 (PDX1), also known as IDX1/IPF1/STF1. PDX1 is expressed in pancreatic buds in the endoderm prior to morphological development of the pancreas [3,4] and has been shown to play a fundamental role in regulating pancreatic development. Gene disruption of PDX1 has been shown to inhibit pancreatic bud maturation and outgrowth, resulting in complete absence of the pancreas [5]. In addition, conditional inactivation of PDX1 in insulin-producing cells results in a progressive loss of β cells, suggesting PDX1 to play an essential role in maintaining β cells [6].

Therefore, to generate insulin-producing cells, several groups have overexpressed PDX1 in various sites [7–11]. Adenovirus-mediated transfer of the PDX1 gene reportedly ameliorates streptozotocin (STZ)-induced hyperglycemia in a short time (within 10 days) [7] as well as for longer periods [12] via production of insulin in the liver. However, helper-dependent adenovirus (HDAD)-mediated PDX1 gene transfer into the liver reportedly results in severe hepatitis and functional failure due to production of pancreatic exocrine enzymes [10]. In addition, transgenic mice overexpressing PDX1 in the liver also develop liver failure [11].

PDX1 has been shown to activate target genes by association with several co-factors such as PBX [13] and the expressions of these protein partners are absent in the liver. To produce a version of PDX1 that would activate target genes without the need for protein partners, the VP16 activation domain from herpes simplex virus was fused to the C-terminus of PDX1 (PDX1-VP16). In PDX1-VP16 transgenic *Xenopus* tadpoles, part or all of the liver is converted to pancreatic tissue, while hepatic differentiation products are lost from the regions converted to pancreas [14].

Therefore, in the present study, we prepared PDX1-VP16 adenovirus and compared the effects of PDX1-VP16 expression with those of wt-PDX1 in the adult murine liver in vivo. These recombinant adenoviruses were administered at a titer of 2×10^8 pfu, which is one to two orders of magnitude lower than those used in previous reports [7,12]. Herein we demonstrate PDX1-VP16 gene transduction to induce hepatocytic production of insulin, but not glucagon or amylase, more efficiently than wt-PDX1, resulting in reversal of STZ-induced hyperglycemia. We found that PDX1-VP16 gene therapy induced endogenous PDX1 expression in the liver, and hence sustained expression of insulin. In contrast to transgenic tadpole experiments, the conversion was partial and liver-specific gene expressions including those of albumin and transferrin were maintained in insulin-producing cells.

Materials and methods

Recombinant adenoviruses. Murine PDX1 cDNA was cloned from a MIN6 cDNA library by PCR. Using PCR, the *Cla*I site was added to murine PDX1 cDNA, which was digested with *Cla*I and subcloned into VP16-N (kind gift from Dr. H. Kanamori) as described [14]. Recombinant adenoviruses containing wt-PDX1 and PDX1-VP16 cDNA were prepared as reported previously [15–17]. LacZ adenovirus was used as a control [18].

Animals. Male C57BL/6N mice were purchased from Clea (Tokyo, Japan), housed in an air-conditioned environment, with a 12-h light-dark cycle, and fed a regular unrestricted diet. Diabetes was induced by intraperitoneal injection of 160–170 mg/kg STZ (Sigma St. Louis, MO) in citrate buffer at 5–6 weeks of age. Blood glucose was determined after a 10 h fast at 6 days after STZ injection; mice with fasting glucose levels of 300–600 mg/dl were used for the experiments. The mice were treated with 2×10^8 plaque-forming units of recombinant adenovirus by systemic injection into the tail vein and killed 40 days after adenovirus injection. Serum insulin concentrations were measured using a rat insulin ELISA Kit Ultra Sensitive (Morinaga, Tokyo, Japan).

Oral glucose tolerance tests. Oral glucose tolerance tests were performed 40 days after adenovirus infusion. Serum glucose levels were determined before, and 15, 30, 60, 90, and 120 min after, administration of oral glucose (1 g/kg body weight).

Immunoblotting. Liver samples were homogenized in buffer (100 mM Tris, pH 8.5, 250 mM NaCl, 1% BP-40, and 1 mM EDTA). Tissue homogenates were centrifuged at 14,000*g* for 10 min at 4 °C. Supernatants including tissue protein extracts (180 μg total protein) were then boiled in Laemmli buffer containing 10 mM dithiothreitol. Aliquots of proteins (15 μg) were subjected to SDS–PAGE. Immunoblot analyses were performed using ECL plus a Western Blotting Detection System Kit (Amersham Buckinghamshire, UK). Antibodies to PDX1 (A-17, Santa Cruz Biotechnology, Santa Cruz, CA) and HSV-1 VP16 (vA-19, Santa Cruz Biotechnology) were commercially obtained.

Immunohistochemistry. Livers of mice were excised 40 days after adenoviral treatment and fixed overnight in 10% paraformaldehyde. Fixed tissues were processed for paraffin embedding and 3 μm sections were prepared. For immunohistochemistry, the streptavidin–biotin (SAB) method was performed using a Histofine SAB-PO kit (Nichirei, Tokyo, Japan) for insulin, glucagon, and amylase, and a MAX-PO kit (Nichirei) for somatostatin, and an EnVision kit/HRP (DAKO, Glostrup, Denmark) for pancreatic polypeptide. Slides were deparaffinized, and then were either autoclaved in citrate buffer for antigen retrieval before being incubated in blocking solution (for amylase, somatostatin, and pancreatic polypeptide detection), or immediately exposed to the blocking solution (for insulin and glucagon detection). For insulin detection, sections were incubated for 18 h at 4 °C with monoclonal antibody against human insulin (Sigma) diluted 1:1000 in PBS. For detection of glucagon, sections were incubated for 18 h at 4 °C with antiserum raised against human glucagon (DAKO) diluted 1:3000 in PBS. For detection of somatostatin, sections were incubated overnight at 4 °C with rat anti-somatostatin monoclonal antibody (Chemicon, Temecula, CA) diluted 1:100 in PBS. For detection of pancreatic polypeptide, sections were incubated overnight at 4 °C with antiserum raised against rat pancreatic polypeptide (LINCO, St. Charles, MO) diluted 1:100 in PBS. For detection of amylase, sections were incubated for 18 h at 4 °C with antiserum raised against the C-terminus of human amylase (Santa Cruz Biotechnology) diluted 1:1000 in PBS. Slides were then incubated with the biotinylated IgG for 1 h and next with peroxidase-conjugated streptavidin for 30 min at room temperature. Finally, immunoreactivity was visualized by incubation with a substrate solution containing 3,3′-diaminobenzidine tetrahydrochloride (DAB).

Fluorescent immunocytochemistry. The 3 μm sections of paraffin-embedded liver were processed as follows. For double staining of

insulin and transferrin or albumin, the sections were incubated overnight with antibodies against insulin and transferrin (goat polyclonal; Santa Cruz Biotechnology) or albumin (rabbit polyclonal; Biogenesis, Kingston, New Hampshire) at 4 °C. Antibodies against insulin, transferrin, and albumin were diluted 1:1000, 1:5000, and 1:5000, respectively, in PBS. For double staining of insulin and transferrin, the sections were then incubated for 1 h at room temperature in a mixture of TRITC-conjugated sheep anti-mouse IgG and FITC-conjugated donkey anti-goat IgG (Jackson Immuno Research, West Grove, PA) diluted 1:1000 in PBS. For double staining of insulin and albumin, the sections were incubated in a mixture of Alexa Fluor 488 goat anti-mose IgG (Molecular Probes, Eugene, OR) and Alexa Fluor 546 goat anti-rabbit IgG diluted 1:1000 in PBS. Sections were observed under a fluorescence microscope (Leica DM RXA, Leica Microsystems, Wetzlar, Germany). The image was analyzed with a Q-fluoro analyzing system (Leica).

Results

To express a PDX1 mutant, in the liver, which is constitutively active without association with protein partners, we prepared a recombinant adenovirus encoding the VP16 activation domain from herpes simplex virus [19,20] fused to the C-terminus of murine PDX1 (PDX1-VP16). For comparison, we also prepared recombinant adenoviruses encoding the wild-type PDX1 (wt-PDX1) and LacZ. These recombinant adenoviruses, at 2×10^8 pfu, were injected intravenously 6 days after STZ administration, when hyperglycemia had already developed; blood glucose levels after a 10 h fast were approximately 400 mg/dl (Fig. 1B). Mice given the LacZ adenovirus were used as controls (LacZ-mice). Systemic infusion of recombinant adenoviruses into mice through the tail vein caused transgene expression primarily in the liver, with no detectable expression in peripheral tissues such as muscle, fat, kidney or brain (data not shown), as reported previously [21].

As shown in Fig. 1A, immunoblotting of hepatic lysates on day 3 after adenoviral administration with anti-PDX1 antibody revealed that ectopic expression of wt-PDX1 or PDX1-VP16 was obtained in the liver. Administration of recombinant adenoviruses at the same titer induced similar levels of PDX1 protein expression.

We next examined the effects of treatment with these adenoviruses on STZ-induced hyperglycemia (Fig. 1B). Administration of wt-PDX1 adenovirus did not significantly decrease fasting blood glucose levels through day 20. Although, interestingly, fasting blood glucose levels were slightly but significantly decreased after day 30 as compared with those in STZ-treated LacZ-mice, administration of wt-PDX1 adenovirus at such a low titer exerted only very small effects in terms of reversal of hyperglycemia.

In contrast, administration of PDX1-VP16 adenovirus more effectively reversed STZ-induced hyperglycemia (Fig. 1B). Hepatic expression of PDX1-VP16 induced significant, profound decreases in fasting blood glucose levels. Although fasting blood glucose levels rose slightly between day 10 and day 15, the therapeutic effects were sustained throughout the experiments. As shown in Table 1, some variation in results was observed. Thirteen percent of PDX1-VP16-mice exhibited almost no decrease in blood glucose levels, although the proportion of these mice was significantly lower than that of wt-PDX1-mice. In contrast, in 27% of PDX1-VP16-mice, fasting blood glucose levels were lower than 200 mg/dl. No such normalization of glucose levels was obtained by wt-PDX1 adenovirus administration (Table 1). Thus, PDX1-VP16 expression in the liver more effectively lowered blood glucose levels and these effects persisted even after adenoviral-mediated gene expression had declined.

To examine the mechanism whereby administration of PDX1-VP16 adenovirus efficiently and persistently lowered blood glucose levels in STZ-treated mice, liver sections from these mice on day 40 after adenoviral administration were immunostained with anti-insulin antibody (Fig. 1C). No insulin staining was detectable in the livers of LacZ-mice. In wt-PDX1-mice, very faint staining with anti-insulin antibody was detected in the liver. In contrast, in PDX1-VP16 mice, strong insulin staining was detected in the cytoplasm of hepatocytes in scattered portions of the liver. The insulin positive cells were seen mostly around vessels. The scant residual insulin-positive cells in the pancreas did not differ significantly among these mice (data not shown). Thus, insulin secretion from hepatocytes is likely to contribute to lowering blood glucose levels in PDX1-VP16-mice.

To confirm that the hepatocytes were secreting insulin, serum levels of immunoreactive insulin in these mice on day 40 after adenoviral administration were measured. In LacZ-mice, STZ treatment induced severe insulinopenia: fasting serum insulin levels were less than 40 pg/ml (Fig. 1D), resulting in severe hyperglycemia. Adenoviral administration of the wt-PDX1 gene slightly increased serum insulin levels. In contrast, PDX1-VP16 adenoviral administration resulted in a substantial increase in serum insulin levels, i.e., more than 6-fold (Fig. 1D). On the other hand, fasting serum insulin levels in the control C57Bl/6N mice of the same age, without STZ treatment, were 340.7 ± 29.9 pg/ml ($n = 6$). Thus, hepatic PDX1-VP16 expression improved fasting serum insulin levels to approximately two-thirds those in normal mice. These data suggest that transient PDX1-VP16 expression in the liver exerted sustained and stronger effects in terms of production and secretion of insulin as compared with wt-PDX1 expression, resulting in the reversal of STZ-induced hyperglycemia.

Oral glucose tolerance tests were performed using LacZ-mice, wt-PDX1-mice, and PDX1-VP16-mice on day 40 (Fig. 2A). STZ-treated LacZ-mice exhibited hyperglycemia: more than 450 mg/dl throughout the

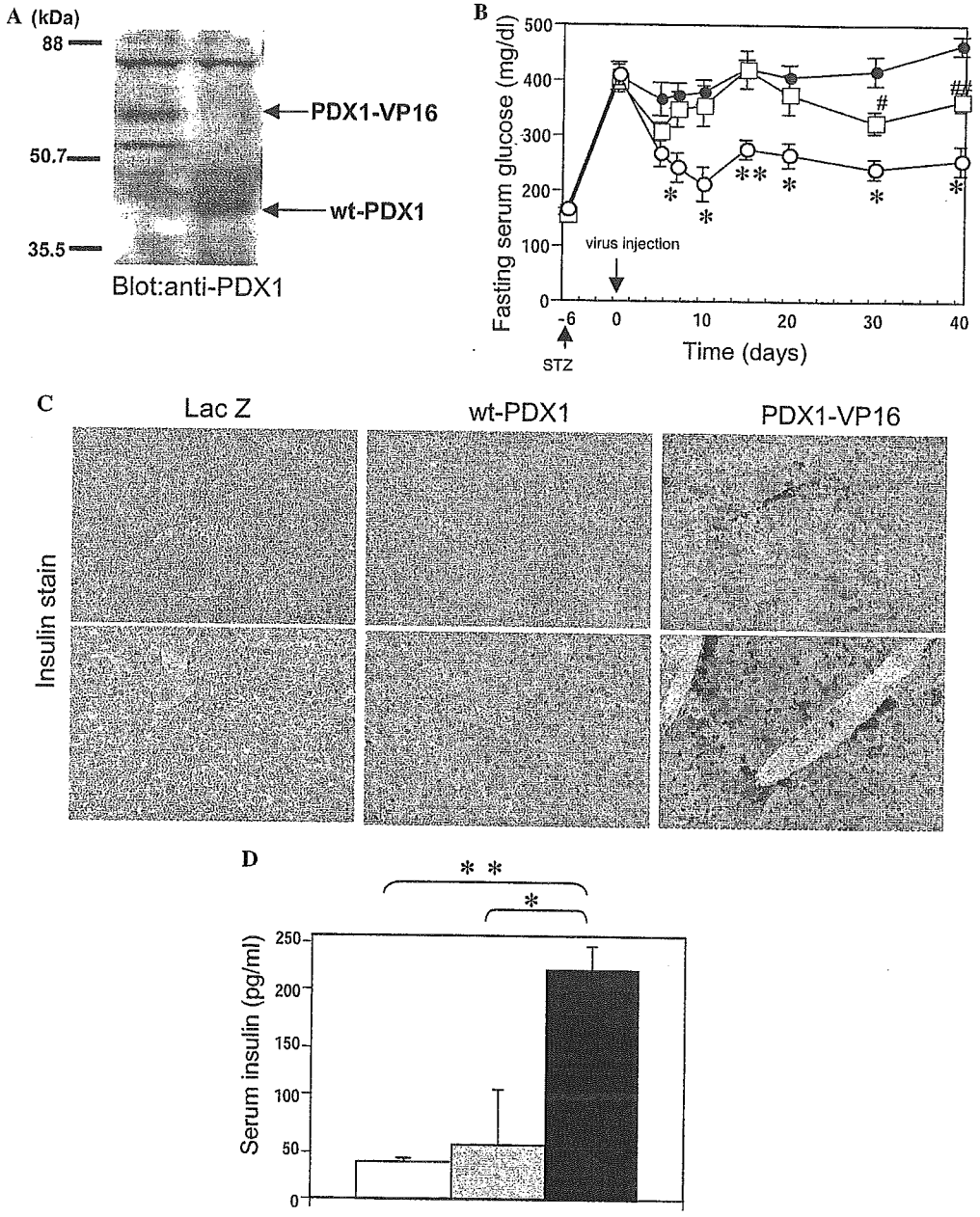

Fig. 1. Effects of wt-PDX1 and PDX1-VP16 adenoviral gene therapy on STZ-induced diabetic mice. (A) Liver lysates from STZ-mice infused with 2×10^8 pfu/body of adenovirus containing wt-PDX1 (left lane) or PDX1-VP16 (right lane) were immunoblotted with anti-PDX1 antibody. (B) Fasting blood glucose levels of STZ-mice treated with LacZ adenovirus (closed circle; $n = 13$), wt-PDX1 adenovirus (open square; $n = 8$) or PDX1-VP16 adenovirus (open circle; $n = 15$). Amount of injected adenoviruses was 2×10^8pfu/body in all experiments. (C) Liver sections from LacZ-mice (left panels), wt-PDX1-mice (middle panels), and PDX1-VP16-mice (right panels) on day 40 after adenoviral treatment were immunostained with anti-insulin antibody. Original magnification 100× (upper panels) and 200× (lower panels). (D) Fasting serum insulin levels 40 days after adenoviral treatment with LacZ (open bar; $n = 7$), wt-PDX1 (gray bar; $n = 8$), or PDX1-VP16 (black bar; $n = 7$) adenovirus. Data are presented as means ± SEM. $^*P < 0.05$, $^{**}P < 0.01$ versus wt-PDX1, $^{\#}p < 0.05$, and $^{\#\#}p < 0.01$ versus LacZ, assessed by unpaired t test.

tests. In PDX1-VP16-mice, glucose levels throughout the tests were significantly lower than those in wt-PDX1-mice. The blood glucose levels peaked at 30 min after glucose load and thereafter tended to fall, although the reversal was incomplete at 120 min. These findings suggest that, in PDX1-VP16-mice, glucose-responsive insulin secretion from the liver is involved in lowering post-prandial blood glucose levels but is not enough to rapidly reverse a rise in blood glucose levels after a glucose load, in contrast to that from the pancreas by β cells.

Using HDAD, PDX1 expression in the liver reportedly induces expression of exocrine enzymes in insulin-producing cells in the liver and causes severe hepatitis. It has also been reported that, in transgenic mice expressing PDX1 ectopically in the liver, not only insulin but

Table 1
Distribution of blood glucose levels in each treatment group

Blood glucose (mg/dl)	100–200	200–300	300–400	400–500	500–600
LacZ (%)	0	0	8	69	23
wt-PDX1 (%)	0	12	50	38	0
PDX1-VP16 (%)	27	47	13	13	0

Blood glucose levels were determined 40 days after each adenoviral treatment. Blood glucose levels of mice before the adenoviral treatment (6 days after STZ injection) were all above 300 mg/dl. (Lac Z; $n = 13$, wt-PDX1; $n = 8$, and PDX1-VP16; $n = 15$.)

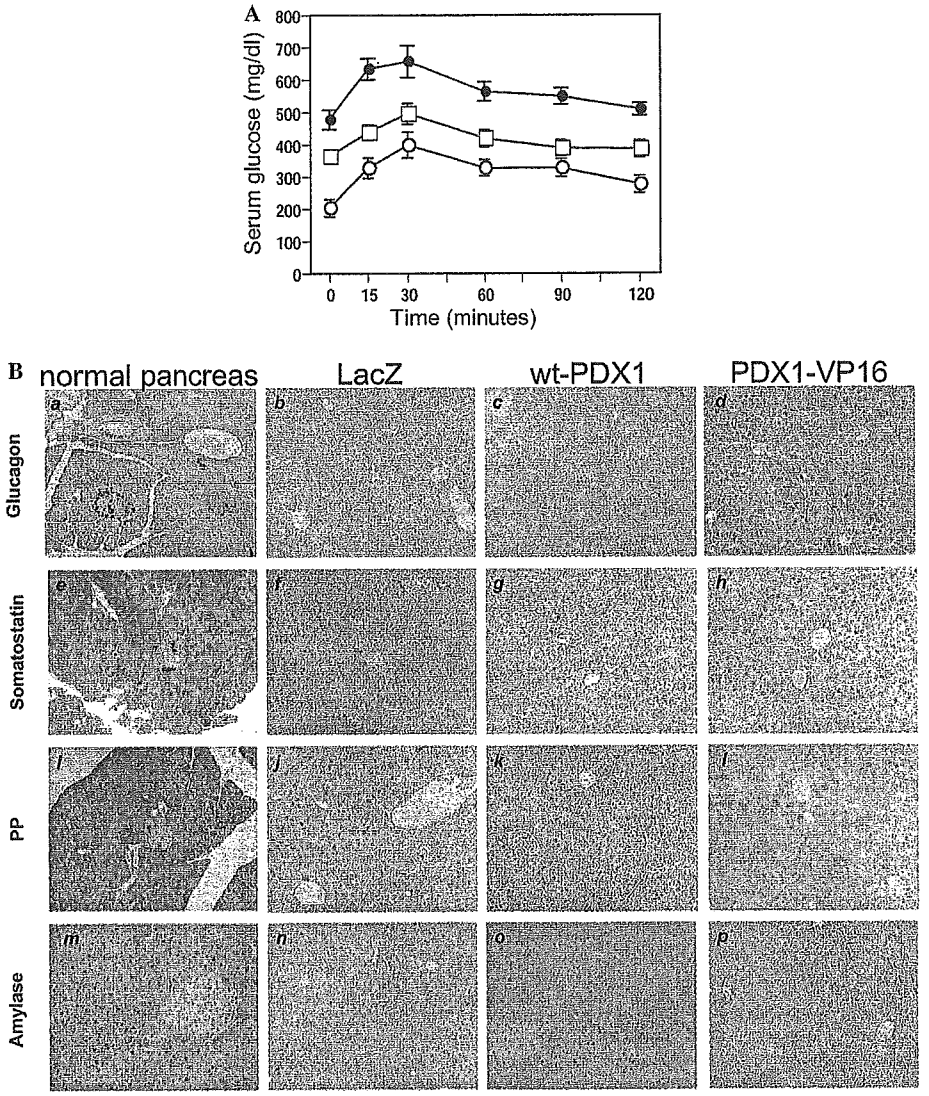

Fig. 2. Effects of wt-PDX1 and PDX1-VP16 adenoviral gene therapy on blood glucose levels after a glucose load, and glucagon, somatostatin, pancreatic polypeptide, and amylase expressions. (A) Blood glucose levels during oral glucose tolerance testing (1 g/kg body weight) in LacZ-mice (closed circle; $n = 7$), wt-PDX1-mice (open square; $n = 8$), and PDX1-VP16-mice (open circle; $n = 7$) on day 40 after adenovirus administration. Data are presented as means ± SEM. (B) immunohistochemical staining of livers from LacZ-mice (b,f,j,n), wt-PDX1-mice (c,g,k,o), and PDX1-VP16-mice (d,h,l,p) with glucagon (b–d), somatostatin (f–h), pancreatic polypeptide (j–l) or amylase (n–p) antibody. Sections of normal pancreas were used as positive controls for each staining procedure (a,e,i,m). Original magnification 100×.

also other endocrine hormones as well as pancreatic exocrine genes are expressed, resulting in dysmorphogenesis and hepatic failure [10]. In contrast, in the present study, adenovirus-mediated transduction of the wt-PDX1 or the PDX1-VP16 gene into the liver did not induce lobe structural abnormalities or substantial infiltration of inflammatory cells (Fig. 2B). Furthermore, using immunohistochemistry, no immunoreactivity against glucagon

or somatostatin was detected in livers from wt-PDX1-mice and PDX1-VP16-mice. In addition, in these livers there was no detectable production of amylase, a pancreatic exocrine enzyme (Fig. 2B), which may explain the normal morphogenesis in our experimental animals. On the other hand, pancreatic polypeptide was expressed in livers from PDX1-VP16-mice, and in those from wt-PDX1-mice though to a lesser extent. These results demonstrate that transient expression of PDX1-VP16 alters the character of hepatocytes to preferentially produce insulin and pancreatic polypeptide, but not other endocrine hormones or exocrine enzymes.

Adenoviral gene transfer induced gene expression for 1 week but, after 2 weeks, this expression reportedly disappeared [22]. However, in the present study, the blood glucose lowering effects and hepatic insulin expression persisted for at least 40 days. Therefore, the time course of PDX1 protein expression levels was examined. As shown in Fig. 3A, immunoblotting using anti-VP16 activation domain antibody revealed PDX1-VP16 protein to be expressed on day 3 but expression was markedly decreased on day 7, and undetectable on day 21. Thus, even after disappearance of VP16-PDX1 expression, hepatocytes expressed insulin, resulting in lowering of blood glucose levels. Interestingly, immunoblotting using anti-PDX1 antibody showed that endogenous PDX1 protein, which had the same molecular weight as wt-PDX1, came to be expressed on day 21. Thus, transient expression of PDX1-VP16 endowed hepatocytes with certain pancreatic β cell features and endogenous PDX1 expression is likely to maintain the insulin-producing function of these cells.

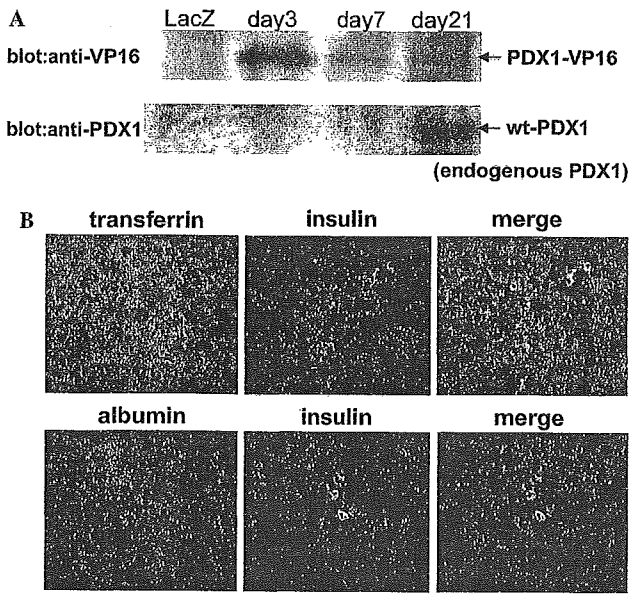

Fig. 3. Treatment with PDX1-VP16 adenovirus induced persistent expression of endogenous PDX1 but albumin and transferrin were co-expressed in insulin-expressing cells. (A) Liver lysates from PDX1-VP16 mice at different time points after adenoviral treatment were immunoblotted with anti-VP16 (upper panel) or anti-PDX1 (lower panel) antibody. (B) Liver sections from PDX1-VP16 mice on day 40 were double-immunostained with insulin (middle panels) and transferrin (upper-left panels) or albumin (lower-left panels) antibodies. Right panels represent the merged images.

To determine whether the insulin-producing cells in the liver had completely transdifferentiated and lost their hepatocytic character, liver sections from PDX1-VP16 mice on day 40 were immunostained with insulin and transferrin (upper panels in Fig. 3B) or albumin (lower panels in Fig. 3B). Fluorescence immunohistochemistry revealed that insulin-producing cells in the liver also expressed transferrin and albumin. Expression levels of these liver-specific proteins were not substantially decreased as compared with non-insulin-producing cells around the insulin-producing cells. These findings suggest functional hepatocyte-specific characteristics are maintained in insulin-producing cells in the liver. Thus, these hepatocytes were not completely converted to pancreatic cells.

Discussion

In the present study, administration of recombinant adenovirus containing an activated form of PDX1 efficiently induced insulin production in hepatocytes, resulting in reversal of STZ-induced hyperglycemia. The effects were sustained even when exogenous protein expression was no longer detectable. In turn, endogenous PDX1 protein came to be expressed in hepatocytes, which is likely to be the mechanism underlying the sustained effects. On the other hand, albumin and transferrin expressions were observed in insulin-producing cells, suggesting the maintenance of hepatocyte-specific characteristics.

Ferber et al. [7] reported that administration of wt-PDX1 adenovirus at 2×10^9 pfu/mouse ameliorates STZ-induced hyperglycemia but the observed period was very short (no more than 10 days). The same research group also reported the long-term effects of PDX1 gene transfer but the titer of recombinant adenovirus used was relatively high ($1–5 \times 10^{10}$ pfu/mouse) [12]. Such high titers may result in liver damage due to adenoviral toxicity. In the present study, to avoid adenoviral toxicity, recombinant adenoviruses were injected at a titer as low as 2×10^8 pfu. With such a small adenoviral delivery, the wt-PDX1 adenovirus exerted very small effects on insulin and glucose levels, whereas PDX1-VP16 adenovirus substantially increased insulin levels and reversed STZ-induced hyperglycemia. These findings suggest that constitutive activation of PDX1 overcomes the inefficiency associated with low expression levels of PDX1 proteins. Thus, adenoviral transfer of the PDX1-VP16 gene into the liver would presumably be safer than wt-PDX1 gene therapy.

HDAD-mediated PDX1 expression in the liver reportedly causes severe hepatitis including marked inflammatory cell infiltration with focal necrosis associated with expression of pancreatic exocrine genes [10]. In addition, conditional transgenic mice generated by crossing CAG-CAT-PDX1 mice with alb-Cre recombinase-mice also displayed functional liver failure with hepatic expression of exocrine enzymes [11]. In these two models, exogenous PDX1 expression is persistent. Transgenes delivered by HDADs are expressed for long periods exceeding several months. In conditional transgenic mice [11], cells, in which the albumin promoter had once been activated, permanently expressed PDX1 driven by the CAG promoter. These findings suggest that high and persistent expression of PDX1 induces exocrine enzyme expression and thereby liver failure. In the present study, exogenous gene expressions of wt-PDX1 and PDX1-VP16 were transient and expression levels were relatively low on day 7 (Fig. 3A). Thus, transient expression appears to be important for endowing hepatocytes with certain features of pancreatic β cells, but not of exocrine cells.

It is noteworthy that exogenous, transient expression of PDX1-VP16 induced prolonged expression of endogenous PDX1 which apparently contributed to persistent insulin production with hepatocytic features. Ber et al. also reported that rat PDX1 gene transduction using first-generation adenovirus induced persistent endogenous (murine) PDX1 expression. Thus, transient expression of wt-PDX1, and more efficiently PDX1-VP16, may induce persistent and low-level expression of endogenous PDX1. In the adult pancreas, persistent but low-level expression of PDX1 is detected only in β cells [3] and PDX1 expression is required for maintaining normal pancreatic β cell function [6]. These observations suggest that persistent, low-level expression of PDX1 is involved in preferential production of insulin and pancreatic popypeptide in hepatocytes.

In transgenic *Xenopus* tadpoles expressing Xlhbox8 (*Xenopus* homolog of PDX1) carrying the VP16 activation domain under a transthyretin promoter, part or all of the liver is reportedly converted to pancreatic tissue without expression of liver-specific gene products, suggesting complete conversion of hepatocytes to pancreatic cells [14]. In contrast, in the present study, insulin-producing cells in the liver in PDX1-VP16 mice also expressed albumin and transferrin, which suggests preservation of hepatocytic functions. This discrepancy may be explained by the differences between amphibian and mammalian cells. Alternatively, the conversion may occur during embryonic differentiation, while, in adult and differentiated hepatocytes, complete transdifferentiation into pancreatic endocrine or exocrine cells would be difficult to achieve even with PDX1-VP16 expression. Although intensive research is necessary to unravel the precise mechanisms underlying transdifferentiation, the partial conversion induced by PDX1-VP16 expression in adult hepatocytes has practical applications, since loss of hepatocytic functions may result in liver failure. Furthermore, incomplete transdifferentiation could prevent the generated insulin-producing cells from being attacked by a destructive autoimmune response in type 1 diabetics.

Acknowledgments

We thank Dr. H. Kanamori (University of Tokyo) for the generous gift of the VP16 gene. We also thank Ms. I. Sato, K. Kawamura, and M. Hoshi for technical support. This work was supported by a Grant-in-Aid for Scientific Research (B2, 15390282), a Grant-in-Aid for Exploratory Research (15659214) to H. Katagiri, and a Grant-in-Aid for Scientific Research (13204062) to Y. Oka from the Ministry of Education, Science, Sports and Culture of Japan. This work was also supported by Tohoku University 21st Century COE Program "CRESCENDO" to J. Imai, J. Gao, and H. Katagiri.

References

[1] A.M. Shapiro, J.R. Lakey, E.A. Ryan, G.S. Korbutt, E. Toth, G.L. Warnock, N.M. Kneteman, R.V. Rajotte, Islet transplantation in seven patients with type 1 diabetes mellitus using a glucocorticoid-free immunosuppressive regimen, N. Engl. J. Med. 343 (2000) 230–238.

[2] G. Deutsch, J. Jung, M. Zheng, J. Lora, K.S. Zaret, A bipotential precursor population for pancreas and liver within the embryonic endoderm, Development 128 (2001) 871–881.

[3] H. Ohlsson, K. Karlsson, T. Edlund, Ipf1, a homeodomain-containing transactivator of the insulin gene, EMBO J. 12 (1993) 4251–4259.

[4] M.F. Offield, T.L. Jetton, P.A. Labosky, M. Ray, R.W. Stein, M.A. Magnuson, B.L. Hogan, C.V. Wright, Pdx-1 is required for pancreatic outgrowth and differentiation of the rostral duodenum, Development 122 (1996) 983–995.

[5] J. Jonsson, L. Carlsson, T. Edlund, H. Edlund, Insulin-promoter-factor 1 is required for pancreas development in mice, Nature 371 (1994) 606–609.

[6] U. Ahlgren, J. Jonsson, L. Jonsson, K. Simu, H. Edlund, Beta-cell-specific inactivation of the mouse ipf1/pdx1 gene results in loss of the beta-cell phenotype and maturity onset diabetes, Genes Dev. 12 (1998) 1763–1768.

[7] S. Ferber, A. Halkin, H. Cohen, I. Ber, Y. Einav, I. Goldberg, I. Barshack, R. Seijffers, J. Kopolovic, N. Kaiser, A. Karasik, Pancreatic and duodenal homeobox gene 1 induces expression of insulin genes in liver and ameliorates streptozotocin-induced hyperglycemia, Nat. Med. 6 (2000) 568–572.

[8] A. Grapin-Botton, A.R. Majithia, D.A. Melton, Key events of pancreas formation are triggered in gut endoderm by ectopic expression of pancreatic regulatory genes, Genes Dev. 15 (2001) 444–454.

[9] R.S. Heller, D.A. Stoffers, M.A. Hussain, C.P. Miller, J.F. Habener, Misexpression of the pancreatic homeodomain protein idx-1 by the hoxa-4 promoter associated with agenesis of the cecum, Gastroenterology 115 (1998) 381–387.

[10] H. Kojima, M. Fujimiya, K. Matsumura, P. Younan, H. Imaeda, M. Maeda, L. Chan, Neurod-betacellulin gene therapy induces islet neogenesis in the liver and reverses diabetes in mice, Nat. Med. 9 (2003) 596–603.
[11] T. Miyatsuka, H. Kaneto, Y. Kajimoto, S. Hirota, Y. Arakawa, Y. Fujitani, Y. Umayahara, H. Watada, Y. Yamasaki, M.A. Magnuson, J. Miyazaki, M. Hori, Ectopically expressed pdx-1 in liver initiates endocrine and exocrine pancreas differentiation but causes dysmorphogenesis, Biochem. Biophys. Res. Commun. 310 (2003) 1017–1025.
[12] I. Ber, K. Shternhall, S. Perl, Z. Ohanuna, I. Goldberg, I. Barshack, L. Benvenisti-Zarum, I. Meivar-Levy, S. Ferber, Functional, persistent, and extended liver to pancreas transdifferentiation, J. Biol. Chem. 278 (2003) 31950–31957.
[13] S. Dutta, M. Gannon, B. Peers, C. Wright, S. Bonner-Weir, M. Montminy, Pdx:Pbx complexes are required for normal proliferation of pancreatic cells during development, Proc. Natl. Acad. Sci. USA 98 (2001) 1065–1070.
[14] M.E. Horb, C.N. Shen, D. Tosh, J.M. Slack, Experimental conversion of liver to pancreas, Curr. Biol. 13 (2003) 105–115.
[15] H. Mizuguchi, M.A. Kay, Efficient construction of a recombinant adenovirus vector by an improved in vitro ligation method, Hum. Gene Ther. 9 (1998) 2577–2583.
[16] H. Mizuguchi, M.A. Kay, A simple method for constructing e1- and e1/e4-deleted recombinant adenoviral vectors, Hum. Gene Ther. 10 (1999) 2013–2017.
[17] T. Anno, S. Uehara, H. Katagiri, Y. Ohta, K. Ueda, H. Mizuguchi, Y. Moriyama, Y. Oka, Y. Tanizawa, Overexpression of constitutively activated glutamate dehydrogenase induces insulin secretion through enhanced glutamate oxidation, Am. J. Physiol. Endocrinol. Metab. 286 (2004) E280–E285.
[18] H. Katagiri, T. Asano, H. Ishihara, K. Inukai, Y. Shibasaki, M. Kikuchi, Y. Yazaki, Y. Oka, Overexpression of catalytic subunit p110alpha of phosphatidylinositol 3-kinase increases glucose transport activity with translocation of glucose transporters in 3t3-l1 adipocytes, J. Biol. Chem. 271 (1996) 16987–16990.
[19] I. Sadowski, J. Ma, S. Triezenberg, M. Ptashne, Gal4-vp16 is an unusually potent transcriptional activator, Nature 335 (1988) 563–564.
[20] S.J. Triezenberg, R.C. Kingsbury, S.L. McKnight, Functional dissection of vp16, the trans-activator of herpes simplex virus immediate early gene expression, Genes Dev. 2 (1988) 718–729.
[21] Y. Ishigaki, S. Oikawa, T. Suzuki, S. Usui, K. Magoori, D.H. Kim, H. Suzuki, J. Sasaki, H. Sasano, M. Okazaki, T. Toyota, T. Saito, T.T. Yamamoto, Virus-mediated transduction of apolipoprotein e (apoe)-sendai develops lipoprotein glomerulopathy in apoe-deficient mice, J. Biol. Chem. 275 (2000) 31269–31273.
[22] M.J. Peeters, G.A. Patijn, A. Lieber, L. Meuse, M.A. Kay, Adenovirus-mediated hepatic gene transfer in mice: comparison of intravascular and biliary administration, Hum. Gene Ther. 7 (1996) 1693–1699.

THE JOURNAL OF BIOLOGICAL CHEMISTRY
Vol. 280, No. 18, Issue of May 6, pp. 18525–18535, 2005
Printed in U.S.A.

A Novel Protein Kinase B (PKB)/AKT-binding Protein Enhances PKB Kinase Activity and Regulates DNA Synthesis*

Received for publication, January 18, 2005
Published, JBC Papers in Press, March 7, 2005, DOI 10.1074/jbc.M500586200

Motonobu Anai‡, Nobuhiro Shojima§, Hideki Katagiri¶, Takehide Ogihara¶, Hideyuki Sakoda‡, Yukiko Onishi‡, Hiraku Ono‡, Midori Fujishiro§, Yasushi Fukushima§, Nanao Horike‖, Amelia Viana‖, Masatoshi Kikuchi‡, Noriko Noguchi, Shinichiro Takahashi‡‡, Kuniaki Takata§§, Yoshitomo Oka¶, Yasunobu Uchijima‖, Hiroki Kurihara‖, and Tomoichiro Asano¶¶¶**

*From the ‡Department of Internal Medicine, Institute for Adult Diseases, Asahi Life Foundation, 1-6-1, Marunouchi, Chiyoda-ku, Tokyo 100-0005, Japan, the ¶Division of Molecular Metabolism and Diabetes, Department of Internal Medicine, Tohoku University Graduate School of Medicine, 1-1 Seiryo-cho, Aoba-ku, Sendai, Miyagi 980-8574, Japan, the §§Department of Cell Biology, Institute for Cellular and Molecular Regulation, Gunma University, 3-39-15 Showamachi, Maebashi, Gunma 371-8512, Japan, and the §Department of Internal Medicine, Graduate School of Medicine, **Department of Molecular Biology and Medicine, Research Center for Advanced Science and Technology, ‡‡Department of Animal Sciences, Graduate School of Agriculture and Life Sciences, and ‖Department of Physiological Chemistry and Metabolism, Graduate School of Medicine, University of Tokyo, 7-3-1 Hongo, Bunkyo-ku, Tokyo 113-8655, Japan*

Protein kinase B (PKB)/Akt reportedly plays a role in the survival and/or proliferation of cells. We identified a novel protein, which binds to PKB, using a yeast two-hybrid screening system. This association was demonstrated not only *in vivo* by overexpressing both proteins or by coimmunoprecipitation of the endogenous proteins, but also *in vitro* using glutathione *S*-transferase fusion proteins. Importantly, this protein specifically associates with the C terminus of PKB but not with other AGC kinases and enhances PKB phosphorylation and kinase activation without growth factor stimulation. Thus, we termed this Akt-specific binding protein APE (Akt-phosphorylation enhancer). Since APE-induced phosphorylation of PKB did not occur in cells treated with wortmannin or LY294002, APE itself is not a kinase but seems to enhance or prolong the phosphoinositide 3-kinase-dependent phosphorylation of PKB. In cells in which APE was suppressed by small interfering RNA, DNA synthesis was significantly reduced with suppression of PKB phosphorylation, suggesting a synergistic role of APE in PKB-induced proliferation. On the other hand, in cells overexpressing both PKB and APE, despite markedly increased basal phosphorylation of PKB, both DNA rereplication and subsequent Chk2 phosphorylation and apoptosis were seen, suggesting the involvement of APE in the regulation of cell cycling replication licensing. Taking these observations together, APE appears to be a novel regulator of PKB phosphorylation. Furthermore, the interaction between APE and PKB, possibly dependent on the expression levels of both proteins, may be a novel molecular mechanism leading to proliferation and/or apoptosis.

The serine/threonine protein kinase PKB[1] (also called Akt) is thought to be a key mediator of signal transduction. Upon growth factor stimulation, a family of lipid kinases known as class 1 phosphoinositide 3-kinases (PI 3-kinases) is recruited to the plasma membrane. PI 3-kinases phosphorylate phosphatidylinositol 4,5-bisphosphate at the D-3 position of the inositol ring, converting it to phosphatidylinositol 3,4,5-trisphosphate. Following the activation of PI 3-kinase, PKBs are recruited to the plasma membrane through direct contact of the pleckstrin homology (PH) domain with phosphatidylinositol 3,4,5-trisphosphate and are phosphorylated at Thr^{308} by PDK1 and at Ser^{473} by PDK2, a kinase of which the molecular structure has not yet been identified (1, 2). AGC kinases other than PKB are also known to be regulated by PI 3-kinase, and PKB acts downstream from PI 3-kinase to regulate numerous biological processes, such as proliferation, antiapoptosis, cell growth, and glucose metabolism (1, 2).

PKB has a wide range of substrates, including GSK-3, FKHR (FoxO1), FKHR-L1 (FoxO3), AFX (FoxO4), and eNOS, all of which have the consensus motif *RXRXX*(S/T) (3, 4). Protein kinases do not generally form stable complexes with their substrates, although PKB has been shown to exist in a stable complex with several of its substrates including MDM2, $p21^{Cip1}$/WAF1, and TSC2 (5–8). It was recently shown that several proteins interact with PKB as function modulators rather than as substrates. In a specific subset of T and B cells, TCL1 interacts with the PH domain of PKB and increases its kinase activity (9). Heat shock protein 90 (Hsp90) was shown to form complexes with Cdc37 and PKB, and PKB was stabilized and protected from dephosphorylation and degradation, resulting in increased kinase activity (10). Carboxyl-terminal modulator protein binds to the carboxyl terminus of PKBα. Carboxyl-terminal modulator protein binding reportedly inhibits the phosphorylation and kinase activity of PKB, and stable expression of carboxyl-terminal modulator protein leads to phenotypic regression of

* This work was supported in part by a grant from Takeda Science Foundation. The costs of publication of this article were defrayed in part by the payment of page charges. This article must therefore be hereby marked "*advertisement*" in accordance with 18 U.S.C. Section 1734 solely to indicate this fact.

¶¶¶ To whom correspondence should be addressed: Dept. of Physiological Chemistry and Metabolism, Graduate School of Medicine, University of Tokyo, 7-3-1 Hongo, Bunkyo-ku, Tokyo 113-8655, Japan. Tel.: 81-3-5841-3603; Fax: 81-3-5803-1874; E-mail: asano-tky@umin.ac.jp.

[1] The abbreviations used are: PKB, protein kinase B; PI, phosphoinositide; PH, pleckstrin homology; GST, glutathione *S*-transferase; PARP, poly(ADP-ribose) polymerase; MTT, 3-[4,5-Dimethylthiazol-2-yl]-2,5-diphenyltetrazolium bromide; GFP, green fluorescent protein; siRNA, small interfering RNA; BrdUrd, bromodeoxyuridine; PKC, protein kinase C.

a v-Akt transformed lung epithelial cell line to wild type (11). TRB3 was also identified as a negative modulator of the PKB type (12), although a contradictory report was very recently published (13). These results indicate that understanding PKB modulation is important for elucidating the mechanism of PKB activation and its regulation of cellular functions.

In this study, we identified a novel protein that interacts with PKB (*in vivo* and *in vitro*). Without growth factor stimulation, overexpression of this protein markedly enhances phosphorylation of Thr^{308} and Ser^{473} in PKB, leading to its kinase activation and phosphorylation of its downstream substrates such as GSK-3 and FKHR. In addition, suppression of APE using RNA interference significantly reduces PKB phosphorylation and PKB kinase activity. Therefore, we termed this protein APE (Akt-phosphorylation enhancer) and herein demonstrate the possible role of APE in DNA synthesis and apoptosis in cooperation with PKB.

MATERIALS AND METHODS

Yeast Two-hybrid System—The DupLEX-A two-hybrid system (OriGene) was used for screening. We screened a mouse embryonic cDNA library with the pJG4-5 vector with a bait protein corresponding to the full length of mouse PKBα using a pEG202 vector and yeast strain EGY48. The positive clones were selected and assayed for β-galactosidase activity. Plasmid DNAs were isolated from positive clones and co-transformed with bait cDNA or negative control cDNA back into yeast to reconfirm the interaction. A yeast β-galactosidase assay kit (Pierce) was used to measure the protein-protein *in vivo* interaction according to the manufacturer's instructions.

Northern Blotting—Mouse Multiple Tissue Northern blot (Clontech) was used for Northern blotting. APE cDNA corresponding to the 600 bp of the coding region of the C-terminal and 400 bp of the untranslated region was used as a probe.

Antibody against APE—Fragments of the cDNA clone were subcloned into a glutathione *S*-transferase (GST) expression vector (Amersham Biosciences), expressed in BL21 and purified using glutathione-coupled Sepharose beads. Purified GST fusion proteins were injected into rabbits, and antisera were affinity-purified using the respective antigens. APE-C was generated to a fragment of APE encompassing amino acids 1646–1845. APE-N1 corresponded to amino acids 172–372, and APE-N3 to corresponded to 501–601. Polyclonal antibodies to each antigen were affinity-purified, using each GST fusion protein, after removal of GST-specific antibody.

Gene Constructions and Expression System in Yeast and Mammalian Cells—Full-length APE cDNAs were cloned into the pShuttle vector to express these proteins with an adenovirus expression system (Clontech). The expression cassette was excited and subcloned into pAdeno-X vector (Clontech). Adenovirus was cloned, and large scale virus purification from 293T cell lysates was achieved by performing CsCl density gradient centrifugation twice, followed by overnight dialysis as previously described. An adenovirus expression vector for PKBα with a Myc tag at its C terminus had previously been generated (14). PKBβ, the PKBα PH domain (residues 1–106), the PKBα kinase domain (residues 138–418), PKBα kinase and its hydrophobic domain (residues 148–480), and the PKBα hydrophobic domain (residues 418–480) were generated by PCR using PKBα or PKCβ cDNA as described previously (14). SGK1 (residues 98–431), SGK2 (residues 35–333), PKCβ2 (residues 342–673), and PKCε (residues 408–737) were generated by PCR using a mouse testis cDNA template. APE fragments were generated by PCR using full-length cDNAs as templates. The PCR products were cloned into pEG202 or pJG4-5 vectors.

Cell Cultures—HepG2, COS-7, and HeLa cells were from the RIKEN Cell Bank. Cells were maintained in Dulbecco's modified Eagle's medium supplemented with 10% fetal bovine serum under a 5% CO_2 atmosphere at 37 °C.

Immunoblot Analysis—The antibodies used in this study were anti-Myc (Upstate Biotechnology), anti-Akt, anti-phospho-Thr^{308}-Akt, anti-phospho-Ser^{473}-Akt, anti-phospho-Thr^{68}-Chk2, anti-phospho-Ser^{256}-FKHR, anti-phospho-$Ser^{20/9}$-GSK-3α/β, anti-caspase 3, anti-cleaved caspase 3, anti-poly(ADP-ribose) polymerase (PARP), anti-cleaved PARP (Cell Signaling Technology) anti-FLAG and anti-α tubulin (Sigma). For total cell lysates, cells were washed with ice-cold phosphate-buffered saline twice and collected with Laemmli sample buffer containing 100 mM dithiothreitol before separation by SDS-10% to 6% or 10% polyacrylamide gel. Proteins were transferred to nitrocellulose membranes. Immunoblotting was performed with ECL according to the manufacturer's instructions.

In Vivo Association of APE and PKB—HeLa cells were resuspended (4×10^7 cells/ml) in buffer A (10 mM HEPES (pH 7.9), 10 mM KCl, 1.5 mM $MgCl_2$, 0.34 M sucrose, 10% glycerol, 1 mM dithiothreitol, 5 μg/ml aprotinin, 5 μg/ml leupeptin, 0.5 μg/ml pepstatin A, 0.1 mM phenylmethylsulfonyl fluoride). Mouse testis was homogenized with 50 strokes, using a Teflon/glass homogenizer, in 10 volumes of ice-cold buffer A. Triton X-100 (0.1%) was added, and the cells were incubated for 5 min on ice. The supernatant was clarified by high speed centrifugation (15 min, 20,000 × *g*, 4 °C) to remove nuclei, cell debris, and insoluble aggregates. Endogenous PKB and APE in the HeLa cell lysate or mouse testis lysates were immunoprecipitated with 100 μg of immobilized anti-PKB and anti-APE-C antibodies, respectively. One hundred micrograms of immobilized Rabbit IgG were used as a control. The immunoprecipitates were washed four times in buffer A with 0.1% Triton X-100, eluted with elution buffer, electrophoresed, and transferred to nitrocellulose membranes. These filters were subjected to inmmunoblotting using the antibodies against APE and PKB.

In Vitro Association of APE and PKB—cDNAs encoding amino acids 418–480 of mouse PKBα with the Myc tag and amino acids 1646–1845 of mouse APE with the FLAG tag at their C termini were amplified by PCR. These cDNAs were cloned into pGEX-5X-1 and pET-28a vectors, and fusion protein expressions were induced in *E. coli* strain BL21 by the addition of 0.1 mM isopropyl β-D-thiogalactoside. The expressed proteins were purified using GST or His tag, according to the manufacturer's instructions. GST alone, GST-APE fragment fusion protein, and GST-PKB fragment fusion protein were incubated with glutathione-Sepharose 4B beads (Amersham Biosciences) for 3 h at 4 °C followed by extensive washing in NETN buffer (20 mM Tris-HCl, pH 8.0, 100 mM NaCl, 1 mM EDTA, 0.5% Nonidet P-40). An aliquot containing 20 μg of GST alone and GST-APE fragment fusion protein bound to beads were then incubated with the His tag PKB fragment. Similarly, an aliquot containing 20 μg of GST alone and the GST-PKB fragment fusion protein bound to beads were then incubated with the His tag APE fragment. After a 4-h incubation at 4 °C, the beads were washed five times with NETN buffer. The bound proteins were eluted by incubating the beads in SDS loading buffer containing 0.1 M dithiothreitol, electrophoresed, and then immunoblotted using anti-Myc and anti-FLAG antibodies for detection of the His tag PKB fragment and His tag APE fragment, respectively.

Immunoprecipitation and PKB Kinase Assay—Cells were lysed in Nonidet P-40 lysis buffer (50 mM Tris-HCl pH 7.5, 1% Nonidet P-40, 120 mM NaCl, 1 mM EDTA, 50 mM NaF, 40 mM β-glycerophosphate, 0.1 mM Na_3VO_4, 1 mM phenylmethylsulfonyl fluoride, 10 μg/ml aprotinin, 50 μg/ml leupeptin). For co-immunoprecipitation, we incubated protein lysates with primary antibodies overnight at 4 °C followed by incubation with Protein A-Sepharose. Immunoprecipitates were washed three times with Nonidet P-40 lysis buffer. An Akt kinase assay kit (Cell Signaling Technology) was used to measure PKB kinase activity. PKB was immunoprecipitated with anti-Myc antibody and Protein G-Sepharose. PKB kinase activity was detected using GSK-3β recombinant protein as a substrate according to the manufacturer's instructions.

Gene Transduction and in Vivo Phosphorylation of PKB—Mammalian cell lines were infected with adenovirus the day after plating. Purified virus was added directly to the culture medium. Titers of adenovirus for protein overexpression were adjusted so that the expression levels of the Myc-tagged PKBα were similar, irrespective of APE co-expression. Likewise, APE expression levels were adjusted so as to be similar, irrespective of Myc-tagged PKBα co-expression. Experiments were performed 36 h later for *in vivo* phosphorylation. Cells were starved for 12 h with KRB-Hepes buffer (118.5 mM NaCl, 4.7 mM KCl, 2.5 mM $CaCl_2$, 1.2 mM KH_2PO_4, 1.2 mM $MgSO_4$, 24.9 mM $NaHCO_3$, 30 mM HEPES, pH 7.4) containing 20 mg/ml bovine serum albumin. Cells were stimulated by the indicated stimulant in each experiment and, whenever indicated, 1 μM wortmannin or 10 μM LY294002 1 h prior to stimulation.

Gene Silencing by siRNA—Gene silencing was performed by an adenovirus-mediated siRNA method. For silencing of endogenous APE gene expression in HepG2 cells, a sense fragment (GGATCCGCATTA-ACACCCACCCGCTCTTCAAGAGAGAGCGGGTGGGTGTTAATGTT-TTTTCTAGAGAATTC) and an antisense fragment (GAATTCTCTAG-AAAAAACATTAACACCCACCCGCTCTCTCTTGAAGAGCGGGTGG-GTGTTAATGCGGATCC) were used for human APE. These two oligonucleotides were annealed *in vitro*, and the resultant double-stranded DNA fragments were subcloned into the BamHI-EcoRI site of a pSIREN-Shuttle vector. A negative control vector was supplied by Clontech. The expression cassette containing siRNA of APE or the negative control was excited and subcloned into pAdeno-X vector.

A

```
   1  MENEIFTPLLEQFMTSPLVIWVKTFGPLAAGNGTNLDEYVALVDGVFLNQVMLQINPKSE
  61  SQRVNKKVNNDASLRIHNLSILVRQIKFYYQETLQQLIMMPLPDILIIGKNPFSEQGTEE
 121  VKKLLLLLLGCAVQCQKKEEFIEKIQGLDFDTKAAVAAHIQEVTHNQENVFDLQWMEVTD
 181  MSQEDIEPLLKNMVSHLRRLIDERDEHSETIVELSEERDGVHFLPHASSSAQSPCGSPGM
 241  KRTESRQHLSVELADAKAKIRRLRQELEEKTEQLLDCKQELEQIEVELKRLQQENMNLLS
 301  DARSARMYRDELDALREKAVRVDKLESELSRYKERLHDIEFYKARVEELKEDNQVLLETK
 361  TMLEDQLEGTRARSDKLHELEKENLQLKAKLHDMEMERDMDRKKIEELMEENMTLEMAQK
 421  QSMDESLHLGWELEQISRTSELAEAPQKSLGHEVNELTSSKLLKLEMENQSLTKTVEELR
 481  STADSAAGSTSKILKVEKENQRLNKKVEILENEIIQEKQSLQNCQNLSKDLMKEKAQLEK
 541  TIETLRENSERQIKILEQENEHLNQTVSSLRQRSQISAEARVKDIEKENKILHESIKETC
 601  GKLSKIEFEKRQMKKELELYKEKGERAEELENELNHLGKENELLQKKITNLKITCEKLET
 661  LEQENSELERENRKFKKTLDSFKNLTFQLESLEKENSQLDEENLELRRSVESLKCASMRM
 721  AQLQLENKELESEKEQLRKGLELMRASFKKTERLEVSYQGLDTENQRLQKALENSNKKIQ
 781  QLESELQDLEMENQTLQKSLEELKISSKRLEQLEKENKSLEQETSQLEKDKKQLEKENKR
 841  LRQQAEIKDTTLEENNVKIGNLEKENKTLFKEINVYKESCVRLKELEKENKELVKRATID
 901  IKTLVTLREDLVSEKLKTQQMNNDLEKLTHELEKIGLNKERLLHDEQSTDDSRYKLLESK
 961  LESTLKKSLEIKEEKIAALEARLEESTNYNQQLRHELKTVKKNYEALKQRQDEERMVQSS
1021  IPVSGEDDKWGRESQEATRELLKVKDRLIEVERNNATLQAEKQALKTQLKQLETQNNNLQ
1081  AQILALQRQTVSLQEQNTTLQTQNAKLQVENSTLNSQSTSLMNQNAQLLIQQSSLENENE
1141  SIMKEREDLKSLYDALIKDHEKLELLHERQASEYESLISKHGTLKSAHKNLEVEHKDLED
1201  RYNQLLKQKGQLEDLEKMIKTEQEKMLLESKNHEVVASEYKKLCGENDRLNYTYSQLLKE
1261  TEILQMDHKNLKSVLNNSKLEQTRLEAEFSKLKEQYQQLDITSTKLNNQCELLSQLKGNL
1321  EEENRHLLDQIQTLMLQNRTLLEQNMESKDLFHVEQRQYIDKLNELRRQKEKLEEKIMDQ
1381  YKFYDPSPPRRRGNWITLKMRKLIKSKKDINRERQKSLTLTPTRSDSSEGFLQLPHQDSQ
1441  DSSSVGSNSLEDGQTLGTKKSSTMNDLVQSMVLAGGQWTGSTENLEVPDDISTGKRRKEL
1501  GAMAFSTTAINFSTVNSSAAFRSKQLVNNKDTTSFEDISPQGISDDSSTGSRVHASRPAS
1561  LDSGRTSTSNSNNNASLHEVKAGAVNIQSRPQSHSSGDFSLLHDHETWSSSGSSPIQYLK
1621  RQTRSSPMLQHKISETIESRAHHKMKAGSPGSEVVTLQQFLEESNKLTSIQLKSSSQENL
1681  LDEVMKSLSVSSDFLGKDKPVSCTLARSVSGKTPGDFYDRRTTKPEFLRTGPQKTEDAYT
1741  ISSAGKPTPSTQGKIKLVKETSVSRQSKDSNPYATLPRASSVISTAEGTTRRTSIHDFLS
1801  KDSRLPVSVDSSPPTAGSSSTTASNVNKVQESRNSKSRSREQQSS
```

B

FIG. 1. **Structure and sequence of APE.** *A*, amino acid sequence of mouse APE. *B*, cDNA clones of APE isolated from the yeast two-hybrid screen and the fragments (APE-N1, APE-N3, and APE-C identical to pJG4–5/APE) used to generate an APE-specific antibody are shown *aligned below* a representation of full-length APE.

DNA Synthesis—HepG2 cells were maintained in Dulbecco's modified Eagle's medium supplemented with 10% fetal calf serum for 36 h and then transfected with an adenovirus encoding siRNA of APE or the negative control. Seventy-two hours after transfection, culture media were changed to Dulbecco's modified Eagle's medium supplemented with 0.2% bovine serum albumin, and cells were incubated for an additional 24 h. The cells were then incubated with BrdUrd labeling solution for 4 h. Incorporated BrdUrd was detected by cell proliferation ELISA, BrdUrd (colorimetric) (Roche Applied Science).

3-[4,5-Dimethylthiazol-2-yl]-2,5-diphenyltetrazolium Bromide (MTT) Assay—Cellular proliferation was measured by reduction of MTT, which corresponds to the living cell number and metabolic activity (15). Cells were plated at 5×10^4 cells/well in 24-well plates and transfected with adenovirus. After incubation for the indicated time, MTT solution was added to each well. After 1 h of incubation, the reaction was stopped by adding 1 ml of isopropyl alcohol with 0.04 N HCl. The absorbance of each well was measured at 492 and 630 nm using a microplate reader.

Cell Viability Analysis—HepG2 cells and HeLa cells were infected with control GFP, PKB, APE, or both PKB and APE adenoviruses and incubated for the indicated times. Floating cells were recovered from culture medium by centrifugation at 1200 × *g* for 1 min, and adherent cells were harvested by trypsinization. Both the floating and adherent cells were observed for morphologic changes with a light microscope at ×200 magnification. We combined the adherent and floating cells and measured their viability by using a trypan blue dye exclusion assay.

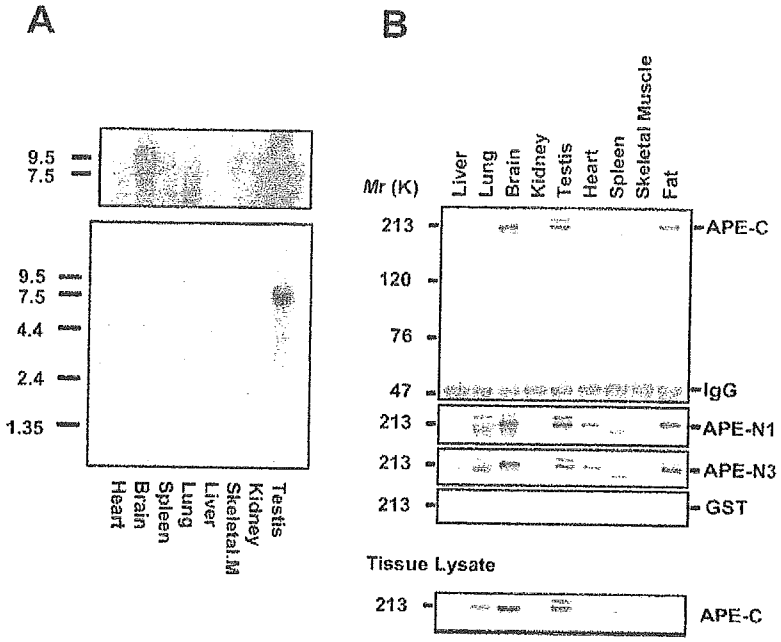

FIG. 2. **Tissue distribution of APE.** *A*, multiple tissue Northern (*MTN*; Clontech) blots probed with 3′ coding and untranslated region of APE. The *upper panel* represents the results of long exposure. *B*, Western analysis of APE. 50 μg of each tissue protein were immunoprecipitated with α-APE-C and immunoblotted with α-APE-C, α-APE-N1, α-APE-N3, and α-GST (*first* to *fourth panels*). Lysates of mouse tissues without immunoprecipitation were also used for immunoblotting with α-APE-C (*bottom panel*). The portions recognized by each antibody are shown under "Materials and Methods" and in Fig. 1.

Cell Cycle Analysis by Flow Cytometry—For cell cycle synchronization, cells were arrested at the G_1-S phase transition separated by two subsequent thymidine blocks (2 mM thymidine) for 14 h, separated by a period of 10 h without thymidine. Both adherent and nonadherent cells were harvested by trypsinization, and an aliquot of 2×10^6 cells was fixed in ice-cold ethanol for at least 1 h at 4 °C. The cells were collected by centrifugation and resuspended in propidium iodine (10 μg/ml) solution containing RNase for analysis of DNA content. Data were then collected on a BD Biosciences FACScan, 20,000 events/sample, using Cellquest software. DNA content analysis was performed with Verity ModFit software for the Macintosh computer.

RESULTS

Cloning of cDNAs Encoding the Protein Binding with PKB—Using full-length mouse PKB as bait in a yeast two-hybrid screen of an embryonic mouse complementary DNA library, we isolated 31 clones displaying β-galactosidase activity. Sequencing analysis revealed 10 of the clones with the strongest β-galactosidase activity to be identical. In all cases, 606 bp of the coding region were followed by a 3′-untranslated region. Isolation of the full-length cDNA by phage screening of the mouse embryonic cDNA library and a series of 5′ rapid amplifications of cDNA ends by PCR showed the largest open reading frame to be 5538 bp, which encode a 1845-amino acid protein with a predicted relative molecular mass (M_r) of 212,478 (Fig. 1*A*, accession number AB087827). By searching several data bases, we found that some mouse clones (BC037020, BC079895, AK129310) and this cDNA to be identical to a mouse homologue of the Kazusa DNA Research Institute clone KIAA1212. This clone is located on mouse chromosome 11 and on human chromosome 2. Although some cDNAs in the data base are presented as "full-length," it seems that they are not, judging from the size of the protein shown in this study. Our mouse cDNA is very likely to be full-length, and this protein was subsequently shown to enhance the phosphorylation of PKB, such that we designated the clone APE (Akt-phosphorylation enhancer). Protein analysis of APE revealed it to be a hydrophilic protein, and that its N terminus has a significant similarity with the putative coiled coil domain of the myosin heavy chain (Fig. 1*B*).

Tissue Distribution of APE—Northern blot analysis detected a 7.9-kb band of APE messenger RNA in the testis (Fig. 2*A*). Longer exposure revealed moderate expression in the brain, and low expressions in the spleen and lungs (Fig. 2*A*, *upper panel*). Anti-APE antibodies were generated against the three different portions of APE (Fig. 1*B*). Immunoblotting with antibodies against APE, irrespective of the differences in the

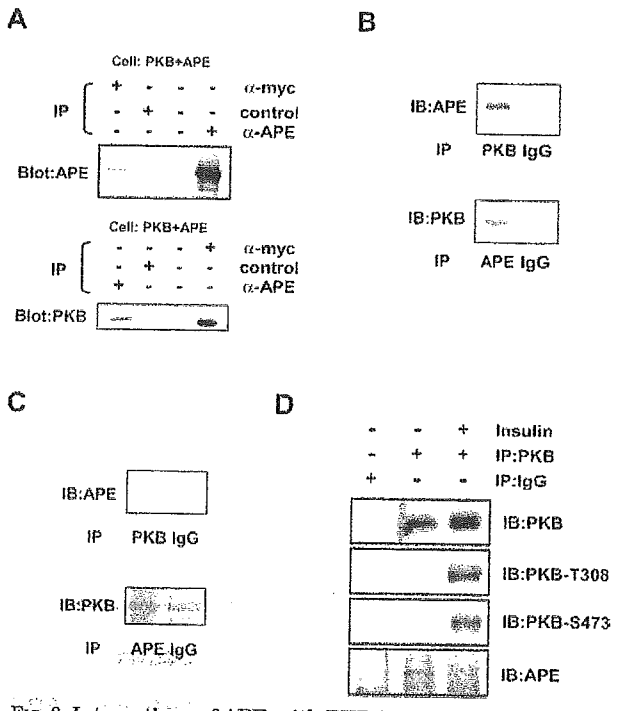

FIG. 3. **Interactions of APE with PKB *in vivo*.** *A*, binding of APE to Myc-PKB. Both APE and Myc-PKB were expressed in COS-7 cells. Immunoprecipitations (*IP*) from cell lysates were performed with the antibodies indicated on the *upper side* of *A*. Immunoblotting (*IB*) using anti-APE-C (*upper panel*) or anti-PKB (*lower panel*) is shown. APE was co-immunoprecipitated with PKB. Endogenous APE and PKB bind *in vivo*. HeLa cells (*B*) or mouse testes (*C*) were homogenized and immunoprecipitated with the antibody indicated *below* the *panels*. APE specifically immunoprecipitated with anti-PKB antibody, and PKB specifically immunoprecipitated with APE antibody. *D*, interaction of APE and PKB was inhibited after insulin stimulation. HEK293 cells were serum starved for 24 h and treated with 100 nM insulin for 15 min. Endogenous PKB were immunoprecipitated with α-PKB monoclonal antibody or with control IgG, and the amount of APE associated with PKB was analyzed by Western blotting.